Type I and III interferons synergize with TNF to promote virally-triggered damage to the intestinal epithelium

Lucie Bernard-Raichon[1,2,3,4]*, Jessica A Neil[1,2,5]*, Kayla Kim[3], Thomas Heaney[1,2], Brittany M Miller[3], Damee Moon[2,6], Ashira Lubkin[2,7,8], Ashley L DuMont[2,9], Victor J Torres[2,9], Jordan Axelrad[10], Yu Matsuzawa-Ishimoto[1,2,11], and Ken Cadwell[1,2,3,12]

1. Kimmel Center for Biology and Medicine at the Skirball Institute, New York University Grossman School of Medicine, New York, NY, USA.
2. Department of Microbiology, New York University Grossman School of Medicine, New York, NY, USA.
3. Division of Gastroenterology and Hepatology, Department of Medicine, University of Pennsylvania Perelman School of Medicine, Philadelphia, PA, USA.
4. Institut de Génomique Fonctionnelle de Lyon, École Normale Supérieure de Lyon, CNRS UMR 5242, UCBL Lyon-1 Lyon F-69007, France.
5. Department of Microbiology and Immunology, Peter Doherty Institute for Infection and Immunity, University of Melbourne, Melbourne, VIC, Australia
6. Institute for Systems Genetics, New York University Grossman School of Medicine, New York, New York, United States
7. Fungal Pathogenesis Section, Laboratory of Clinical Immunology and Microbiology, National Institute of Allergy and Infectious Diseases (NIAID), National Institutes of Health (NIH), Bethesda, MD, USA.
8. Postdoctoral Research Associate program, National Institute of General Medical Sciences, National Institutes of Health (NIH), Bethesda, MD, USA.
9. Department of Host-Microbe Interactions, St. Jude Children's Research Hospital, Memphis, TN, USA.

10. Division of Gastroenterology, Department of Medicine, NYU Grossman School of Medicine, New York, USA.
11. Department of Clinical and Diagnostic Laboratory Science Graduate School of Medical and Dental Science Institute of Science Tokyo (Science Tokyo), Tokyo, Japan
12. Department of Pathobiology, University of Pennsylvania School of Veterinary Medicine, Philadelphia, PA, USA.

* Authors contributed equally to this work

Correspondence to: Ken Cadwell (ken.cadwell@pennmedicine.upenn.edu), Yu Matsuzawa-Ishimoto (matsuzawa.yu@tmd.ac.jp)

Abstract

Excessive cell death in the epithelium due to prolonged immune activation is associated with intestinal diseases such as Crohn's disease. Mice with mutations in the Crohn's disease susceptibility gene *Atg16l1* are susceptible to inflammation associated with intestinal epithelial cell (IEC) death, including loss of antimicrobial Paneth cells triggered by infection with murine norovirus (MNV). Here, we show that intestinal disease downstream of MNV depends on IFN-α/β and IFN-λ signaling in IECs. In mouse organoids, IFNs synergize with TNF to induce RIPK1-dependent cell death, amplified by ATG16L1 deficiency. We further show that human intestinal organoids harboring the *ATG16L1* risk allele exhibit heightened sensitivity to TNF and IFN co-stimulation and to serum from severe COVID-19 patients. Our findings reveal that virally triggered cytokines including IFNs exacerbate epithelial vulnerability in genetically predisposed hosts.

48 **Introduction**

49 A single layer of epithelial cells in the intestine forms the first line of defense against
50 diverse microbial agents ranging from beneficial members of the microbiota to pathogens that
51 cause life-threatening disease (Ramanan & Cadwell, 2016). Intestinal epithelial cells (IECs)
52 include enterocytes that absorb nutrients, chemosensory tuft cells, mucus-secreting goblet cells,
53 and enteroendocrine cells that produce hormones. The small intestinal crypt also harbors Paneth
54 cells, IECs that secrete antimicrobial factors such as lysozyme and defensins. The proper
55 turnover of IECs maintains anatomical integrity and contributes to resolving infections, such as
56 through sloughing of damaged cells bound by adherent or invasive microbes (Churchill et al.,
57 2022). However, inflammatory or excessive cell death triggered by prolonged immune activation
58 is a hallmark of several intestinal diseases including inflammatory bowel diseases (IBDs) such as
59 Crohn's disease (CD) and ulcerative colitis (Patankar & Becker, 2020). The cell death modality,
60 timing, and cell type specificity are likely important variables that contribute to outcomes in
61 infectious and inflammatory diseases of the gut.

62 The etiology of IBDs is complex and associated with genetic and environmental factors
63 (Cadwell & Loke, 2025). Although sustaining remission continues to be a challenge in many
64 patients, the success of therapies that target cytokines and their signaling activities support a
65 disease model in which these soluble immune mediators disrupt the epithelial barrier in a
66 susceptible host. Consistent with this possibility, we demonstrated that mutations in the CD
67 susceptibility gene *ATG16L1* are associated with loss of function and viability of Paneth cells as
68 well as susceptibility to intestinal injury downstream of TNF (Cadwell et al., 2008; Cadwell et al.,
69 2010; Matsuzawa-Ishimoto et al., 2017; Matsuzawa-Ishimoto et al., 2022). ATG16L1 is necessary
70 for the cell biological process of autophagy in which cytosolic material, such as protein aggregates
71 and damaged organelles, is targeted to the lysosome for degradation and recycling (Matsuzawa-
72 Ishimoto et al., 2018). Multiple groups have independently demonstrated that ATG16L1 and other

73 autophagy genes have an epithelial-intrinsic role in promoting intestinal barrier function (Aden et
74 al., 2018; Asano et al., 2017; Benjamin et al., 2013; Conway et al., 2013; Foerster et al., 2023;
75 Jackson et al., 2020; Jung et al., 2019; Matsuzawa-Ishimoto et al., 2020; Matsuzawa-Ishimoto et
76 al., 2017; Patel et al., 2013; Pott et al., 2018; Tschurtschenthaler et al., 2017). Autophagy and
77 related processes may be particularly important in Paneth cells because of their longevity (2-3
78 months) and high secretory burden that make these cells susceptible to ER and mitochondrial
79 stress (Adolph et al., 2013; Bel et al., 2017; Burger et al., 2018; Cadwell et al., 2008; Matsuzawa-
80 Ishimoto et al., 2017).

81 We previously developed a model in which persistent infection with murine norovirus
82 (MNV) of *Atg16l1*-mutant mice, including mice with an IEC-specific deletion of *Atg16l1*
83 (*Atg16l1*$^{fl/fl}$;villin-cre, hereafter referred to as *Atg16l1*$^{\Delta IEC}$), are susceptible to chemical injury to the
84 gut by dextran sodium sulfate (DSS) and develop Paneth cell alterations similar to those observed
85 in patients with CD homozygous for the *ATG16L1 T300A* risk variant (Cadwell et al., 2010;
86 Matsuzawa-Ishimoto et al., 2017). Small intestinal organoids, a 3D cell culture model
87 differentiated from intestinal stem cells, generated from *Atg16l1*-mutant mice or patients with
88 *ATG16L1*^{T300A} undergo necroptosis (programmed necrosis) and loss of Paneth cells upon TNF
89 treatment (Aden et al., 2018; Matsuzawa-Ishimoto et al., 2017). Given that MNV can promote
90 beneficial immune development under certain settings and is otherwise tolerated (Abt et al., 2016;
91 Kernbauer et al., 2014; Neil et al., 2019), the virally-triggered intestinal damage observed in
92 *Atg16l1*$^{\Delta IEC}$ mice provides an opportunity to identify the immune factors that regulate IEC-viability
93 in response to environmental perturbations.

94 Type I Interferons (IFN-α/β) and type III interferons (IFN-λs) are best known for their
95 antiviral functions downstream of Janus kinases (JAK) and signal transducer and activator of
96 transcription proteins (STAT) upon receptor engagement. Although type I and III IFNs induce
97 similar interferon stimulated genes (ISGs), they have distinct activities mediated in part by

98 differential expression of their receptors. In the intestine, the type I IFN receptor (IFNAR) primarily
99 functions in immune cells and is downregulated in IECs in adult mice whereas the type III IFN
100 receptor (IFNLR) is highly produced in IECs and neutrophils (Ingle et al., 2018; Lin et al., 2016;
101 Mahlakoiv et al., 2015). In the context of MNV infection, IFN-α/β prevents extraintestinal
102 dissemination and IFN-λ restricts local replication and fecal shedding (Baldridge et al., 2017; Nice
103 et al., 2015; Nice et al., 2016; Rocha-Pereira et al., 2018; Thackray et al., 2012). Although
104 homeostatic IFN-λ produced by lymphocytes in response to commensal bacteria limits viral
105 replication during early infection (Van Winkle et al., 2022), the viral non-structural protein NS1
106 encoded by persistent strains mediates evasion of IFN-λ to establish prolonged infection of tuft
107 cells (Lee et al., 2017; Wilen et al., 2018). In addition to their antiviral role, IFNs impact intestinal
108 homeostasis. A recent study reported that mice lacking both IFNAR and IFNLR do not survive
109 even low levels of DSS exposure, which was associated with extensive destruction of the colonic
110 epithelium (McElrath et al., 2021). By contrast, IFN-λ levels are high in serum and small intestinal
111 tissue of patients with CD, and over-expression or administration of IFN-λ induces inflammatory
112 forms of epithelial cell death, necroptosis and pyroptosis (Gunther et al., 2019; Jena et al., 2024).

113 Although MNV can activate cell death proteins directly in infected IECs to promote its
114 reproduction and immune evasion (Aktepe et al., 2024; Bok et al., 2009; Deerain et al., 2024;
115 Robinson et al., 2019; Song et al., 2025; Wang et al., 2023), persistent strains display specific
116 tropism for tuft cells due to the restricted expression of the viral entry receptor *Cd300lf* (Graziano
117 et al., 2021; Orchard et al., 2016; Wilen et al., 2018). Thus, in the *Atg16l1* mutant setting, in which
118 cell death is observed in Paneth cells that do not express *Cd300lf*, extracellular factors mediate
119 IEC defects. MNV increases TNF and IFN-γ producing intra-epithelial lymphocytes and inhibits
120 protective γδ T cells upstream of Paneth cell death and DSS-induced disease (Cadwell et al.,
121 2010; Matsuzawa-Ishimoto et al., 2017; Matsuzawa-Ishimoto et al., 2022). Here, we identify a
122 critical cytotoxic role of type I and III IFNs in mediating these effects. We report that deletion of

123 IFNAR or IFNLR in IECs rescues intestinal defects in *Atg16l1* deficient mice and identify a role
124 for IFNs in potentiating TNF-induced cell death. Using organoids and serum from patients with
125 COVID, we provide evidence that the general epithelial cytotoxic effect of cytokines produced in
126 response to viral infections is conserved in humans. Thus, our results suggest that a component
127 of viral sequelae includes production of soluble immune mediators such as TNF and IFNs that
128 compromise the viability of IECs, which is especially detrimental in genetically susceptible hosts.

129

130 **Results**

131 *Epithelial type I and III interferon signaling mediate intestinal damage downstream of viral*
132 *infection.*

133 *Atg16l1*-mutant mice display spontaneous ISG expression in the gut dependent on the
134 microbiota (Marchiando et al., 2013; Martin et al., 2018). To determine whether ISG expression
135 is further increased in the presence of MNV, we examined the small intestine (ileum) and colon
136 of WT and *Atg16l1*$^{\Delta IEC}$ mice 10 days post intragastric inoculation with MNV strain CR6. The levels
137 of three representative ISGs (*Mx2*, *Oasl2*, and *Zbp1*) in the ileum and colon were increased by
138 MNV infection, and for the ileum, highest in MNV-infected *Atg16l1*$^{\Delta IEC}$ mice (Sup. Fig. 1A). IFN-λ
139 is primarily responsible for ISG expression in IECs (Odendall et al., 2014). To confirm that IFN-λ
140 is responsible for the ISG expression, we crossed *Ifnlr* floxed mice to *Atg16l1*$^{\Delta IEC}$ mice to obtain
141 *Atg16l1;Ifnlr*$^{\Delta IEC}$ mice that are deficient in ATG16L1 and IFNLR in IECs. ISG expression in MNV-
142 infected *Atg16l1;Ifnlr*$^{\Delta IEC}$ mice was not significantly different from uninfected Cre-negative
143 controls, hereafter referred to as wild-type (WT) (Sup. Fig. 1A).

144 To determine whether IFN-λ signaling contributes to virally triggered intestinal defects, we
145 examined the susceptibility of *Atg16l1;Ifnlr*$^{\Delta IEC}$ mice to DSS following MNV infection. *Atg16l1*$^{\Delta IEC}$

146 mice showed increased lethality, weight loss, and disease score compared to WT mice upon MNV
147 + DSS treatment (Fig. 1A-C), similar to our previous study (Matsuzawa-Ishimoto et al., 2017). In
148 contrast, these disease readouts were abrogated in MNV + DSS treated *Atg16l1;Ifnlr* $^{\Delta IEC}$ mice
149 and were similar to *Ifnlr*$^{\Delta IEC}$ (*Ifnlr*$^{fl/fl}$villin-cre) and WT controls (Fig. 1A-C). We also generated
150 *Atg16l1;Ifnar*$^{\Delta IEC}$ (*Atg16l1*$^{fl/fl}$*Ifnar*$^{fl/fl}$villin-cre) mice for additional comparison and unexpectedly
151 found that disease was ameliorated. Consistent with a dominant antiviral role of IFNLR at the
152 epithelial barrier during MNV infection (Nice et al., 2015), *Atg16l1;Ifnlr*$^{\Delta IEC}$ mice, but not
153 *Atg16l1;Ifnar*$^{\Delta IEC}$ mice, displayed increased shedding of virus in stool compared to *Atg16l1*$^{\Delta IEC}$ or
154 WT mice (Fig. 1D). None of the mice examined displayed mortality or exacerbated disease in
155 response to DSS in the absence of MNV, except *Atg16l1;Ifnlr*$^{\Delta IEC}$ mice (Sup. Fig 1B). These
156 results indicate that IFNLR and IFNAR in IECs are necessary for the exacerbated intestinal injury
157 response in *Atg16l1;Ifnlr* $^{\Delta IEC}$ mice infected with MNV and may have a different role in uninfected
158 *Atg16l1* mutant mice.

159 We previously showed that Paneth cells are less frequent and structurally altered in the
160 ileum and the colons are shortened in MNV + DSS treated *Atg16l1*$^{\Delta IEC}$ mice (Matsuzawa-Ishimoto
161 et al., 2017). *Atg16l1*$^{\Delta IEC}$ mice displayed a lower number of Paneth cells compared to similarly-
162 treated WT mice, and the remaining Paneth cells showed diffuse lysozyme staining and/or
163 reduced number of lysozyme^{+} granules that are a characteristic of CD (Cadwell et al., 2010).
164 Deleting *Ifnlr* or *Ifnar* in *Atg16l1* $^{\Delta IEC}$ mice failed to fully restore Paneth cells to WT levels, although
165 we note that there was an increase in the number of Paneth cells in *Atg16l1;Ifnar*$^{\Delta IEC}$ mice
166 compared to *Atg16l1*$^{\Delta IEC}$ mice suggesting a partial restoration (Fig. 1E, F). To test potential
167 redundancy, we crossed *Atg16l1;Ifnlr*$^{\Delta IEC}$ mice with *Atg16l1;Ifnar*$^{\Delta IEC}$ mice to generate
168 *Atg16l1;Ifnlr;Ifnar* $^{\Delta IEC}$ mice deficient in both receptors. However, *Atg16l1;Ifnlr;Ifnar* $^{\Delta IEC}$ mice still
169 displayed reductions in Paneth cells and a high proportion showed abnormal lysozyme staining
170 (Fig. 1G). We cannot rule out the possibility that the above analyses would miss Paneth cells that

171 lose their granules, which can happen in the *Atg16l1* mutant setting (Cadwell et al., 2008). To
172 more broadly capture abnormalities, we stained sections for cell death using terminal
173 deoxynucleotidyl transferase–mediated dUTP nick-end labeling (TUNEL). TUNEL-positive cells
174 were rarely detected in the crypts of WT mice whereas a subset of crypts displayed multiple
175 TUNEL-positive cells in *Atg16l1* $^{\Delta IEC}$ mice (Fig. 1E, H, I). Rather than a decrease, the number of
176 TUNEL-positive cells displayed a non-significant increase in *Atg16l1;Ifnar*$^{\Delta IEC}$ mice compared with
177 *Atg16l1* $^{\Delta IEC}$ mice. However, the *Atg16l1;Ifnlr* $^{\Delta IEC}$ mice were similar to WT controls and did not
178 display crypts with >2 TUNEL-positive cells. *Atg16l1;Ifnlr;Ifnar* $^{\Delta IEC}$ mice were similar to *Atg16l1*
179 $^{\Delta IEC}$ mice (Fig. 1E, H). *Atg16l1*$^{\Delta IEC}$ mice also exhibited a shorter colon than WT and *Atg16l1;Ifnlr*
180 $^{\Delta IEC}$ mice following MNV + DSS (Fig. 1I). These results indicate that IFNLR and IFNAR signaling
181 mediate some aspects of disease development in MNV-infected *Atg16l1*$^{\Delta IEC}$ mice including
182 lethality and IEC death but granule alterations in Paneth cells may be involve a more complex
183 role for IFNs.

184

185 *IFNβ and IFNλ exacerbate TNF-mediated cell death of intestinal organoids.*

186 We previously found that organoids generated from *Atg16l1*$^{\Delta IEC}$ mice (*Atg16l1*$^{-/-}$ organoids)
187 display a striking spontaneous ISG signature and that treatment with the JAK inhibitor ruxolitinib
188 prevents TNF-induced cell death of these *Atg16l1*$^{-/-}$ organoids (Matsuzawa-Ishimoto et al., 2020).
189 Although these results are consistent with a role for signaling downstream of cytokine receptors
190 that use the JAK/STAT pathway, it was unclear whether IFNs can cooperate with TNF to induce
191 loss of organoid viability. Because the majority of *Atg16l1*$^{-/-}$ organoids die within the first 2-3 days
192 of seeding when TNF is administered on day 0 (Matsuzawa-Ishimoto et al., 2017), we modified
193 our protocol to increase the dynamic range of the assay and assess the synergistic effect of TNF
194 and IFNs. We found that >50% of *Atg16l1*$^{-/-}$ organoids and ~80% of *Atg16L1*$^{+/+}$ organoids (derived

195 from *Atg16l1*$^{fl/fl}$ mice that were negative for Cre) remained viable 72 hours post-stimulation when
196 TNF was added 3 days after seeding (Fig. 2A, B). Treatment with IFN-β and IFN-λ2 led to similar
197 or slightly greater loss of viability as TNF for both *Atg16L1*$^{+/+}$ and *Atg16l1*$^{-/-}$ organoids (Fig. 2A, B).
198 In contrast, the combination of TNF and IFN led to substantial organoid death. After only 24 h,
199 *Atg16l1*$^{-/-}$ organoids with TNF + IFN-β or TNF + IFN-λ2 resulted in complete loss of viability (Fig.
200 2A, B). *Atg16L1*$^{+/+}$ organoids started to display loss of viability at 24 hours and were completely
201 dead by 48 hours post-treatment with TNF + IFN-β or TNF + IFN-λ2 (Fig. 2A, B). Titration of IFN-
202 β and IFN-λ2 in the presence of TNF showed dose responsiveness and that *Atg16l1*$^{-/-}$ organoids
203 are more sensitive to IFN since 10x less IFN induced same level of cell death in this genotype
204 compared with *Atg16L1*$^{+/+}$ organoids (Fig. 2C). Therefore, IFN-β and IFN-λ2 increase the toxicity
205 of TNF, and ATG16L1 deficiency further sensitizes organoids to the combination of these
206 cytokines.

207 IFN-β can induce TNF production (Aden et al., 2018), which may explain why IFN
208 treatment alone can induce some degree of cytotoxicity to organoids (Fig. 2B). We observed that
209 TNF expression and protein secretion were increased in *Atg16l1*$^{-/-}$ organoids but not *Atg16L1*$^{+/+}$
210 organoids treated with IFN-β (Fig. 2D and Sup. Fig. 2A). Antibody-mediated blockade of TNF
211 rescued viability of *Atg16l1*$^{-/-}$ organoids stimulated with TNF as expected and also greatly
212 improved viability of *Atg16l1*$^{-/-}$ organoids treated with IFN-β (Fig. 2E). Anti-TNF improved viability
213 of *Atg16l1*$^{-/-}$ organoids treated with TNF + IFN-λ2 but not IFN-λ2 alone (Sup. Fig. 2B). These
214 results indicate that IFN-β increases the production of TNF in *Atg16l1*$^{-/-}$ organoids, which
215 contributes to its toxicity.

216 We confirmed the specificity of IFN-β and IFN-λ2 for their cognate receptors. *Atg16l1*$^{-/-}$
217 *Ifnar*$^{-/-}$ organoids were resistant to TNF + IFN-β and *Atg16l1*$^{-/-}$*Ifnlr*$^{-/-}$ organoids were resistant to
218 TNF + IFN-λ2 (Fig. 2F). Also, IFN-β and IFN-λ2 did not induce representative ISGs in the absence
219 of their respective receptors (Sup. Fig. 2C). However, the spontaneous ISG expression observed

220 in untreated *Atg16l1*$^{-/-}$ organoids was absent in *Atg16l1*$^{-/-}$*Ifnlr*$^{-/-}$ but not *Atg16l1*$^{-/-}$*Ifnar*$^{-/-}$ organoids
221 (Sup. Fig. 2C), suggesting a dominant role for IFNLR, possibly due to the overexpression of *Ifnl2*
222 in absence of IFNAR as previously described (Ardanuy et al., 2020). The necroptosis gene *Mlkl*
223 is also an ISG and displayed similar IFNAR and IFNLR dependent expression patterns (Sup. Fig.
224 2C). Given our prior finding that ATG16L1-deficient organoids display spontaneous ISG
225 expression (Matsuzawa-Ishimoto et al., 2020), we determined whether IFN receptor signaling
226 contributed to cell death induced by TNF alone. For these experiments, we added TNF to
227 organoids on day 0, a condition that allows us to examine toxicity of TNF treatment alone.
228 Although the effect of deleting IFNAR or IFNLR individually (*Atg16l1*$^{-/-}$*Ifnar*$^{-/-}$ and *Atg16l1*$^{-/-}$*Ifnlr*$^{-/-}$)
229 was modest, deleting both IFN receptors improved the viability of *Atg16l1*$^{-/-}$ organoids (*Atg16l1*$^{-/-}$
230 *Ifnar*$^{-/-}$*Ifnlr*$^{-/-}$) (Fig. 2G). When these experiments using exogenous cytokines and receptor
231 deletions are taken together, they show that IFNs synergize with TNF to mediate cell death,
232 especially in the ATG16L1-deficient setting.

233

234 *Exacerbation of TNF-induced toxicity in organoids by IFNs is partially dependent on necroptosis*
235 *signaling.*

236 TNF receptor engagement in IECs leads to activation of receptor-interacting
237 serine/threonine protein kinase 1 (RIPK1) to mediate either apoptosis or necroptosis in IECs
238 (Dannappel et al., 2014; Kattah et al., 2018); RIPK1 mediates apoptosis through caspases, and
239 when apoptosis or caspases are inhibited, necroptosis occurs through forming a complex with
240 RIPK3 to phosphorylate the pore forming molecule MLKL that disrupts cell membrane integrity.
241 We and others have shown that TNF-induced cell death in *Atg16l1* deficient intestinal organoids
242 and macrophages is dependent on RIPK1, RIPK3, and MLKL (Aden et al., 2018; Lim et al., 2019;
243 Matsuzawa-Ishimoto et al., 2017). To investigate how the combination of TNF and IFN reduced
244 viability, we treated organoids with ruxolitinib as a control, a pan-caspase inhibitor (QVD), and a

245 RIPK1-inhibitor (Nec1s). Ruxolitinib and Nec1s improved viability of both WT and *Atg16l1*-
246 deficient organoids treated with TNF + IFN-λ2 and TNF + IFN-β (Fig. 3A, B, Sup. Fig. 3A). By
247 contrast, QVD did not improve the viability of TNF + IFN stimulated organoids.

248 We first examined protein levels of cell death mediators at an early time point of cytokine
249 treatment before *Atg16l1*$^{-/-}$ organoids displayed signs of cytotoxicity. Even at 2 h post-stimulation,
250 phosphorylated RIPK3 (pRIPK) and cleaved caspases, especially caspase-3, were visible in TNF
251 or TNF + IFN stimulated *Atg16l1*$^{-/-}$ organoids and not WT organoids (Fig. 3C-F, Sup. Fig. 3B).
252 This result is consistent with the delayed onset of cell death in WT organoids. MLKL and cleaved
253 caspase-3 were detected in WT organoids treated with IFN-λ2 for 24 h, with or without TNF;
254 pMLKL was faintly visible when both cytokines were present (Fig. 3C, D, G, H, Sup. Fig. 3B).
255 Although our earlier observation implicated necroptosis because RIPK1 inhibition and not
256 caspase inhibition protected organoids, we noted the prominent cleavage of caspase-3.
257 Therefore, we tested whether cell death induced by TNF and IFN treatment were dependent on
258 MLKL. *Mlkl*$^{-/-}$ organoids displayed increased viability when treated with TNF + IFN-λ2 or TNF +
259 IFN-β at 24 h, but this protection was less consistent at 48 h (Fig. 3I, H). These results indicate
260 that necroptosis contributes to the loss of viability induced by TNF + IFN treatment of organoids.

261 *Virally-triggered intestinal disease in Atg16l1 mutant mice is RIPK3-dependent.*

262 Paneth cell abnormalities and mortality are ameliorated by RIPK1 inhibition in MNV + DSS
263 treated *Atg16l1*$^{\Delta IEC}$ mice (Matsuzawa-Ishimoto et al., 2017). As a kinase, RIPK3 may also be a
264 targetable molecule. We found that *Atg16l1*$^{\Delta IEC}$*;Ripk3*$^{-/-}$ mice showed substantially reduced
265 lethality and weight loss compared to *Atg16l1*$^{\Delta IEC}$ mice following MNV + DSS treatment and was
266 similar to WT and *Ripk3*$^{-/-}$ control mice (Fig. 4A). Although not a complete reversal, disease score
267 and colon length of *Atg16l1*$^{\Delta IEC}$*;Ripk3*$^{-/-}$ mice were not significantly different from WT and *Ripk3*$^{-/-}$
268 mice (Fig. 4A, B), indicating a general improvement in disease outcomes. In contrast to deletion

269 of IFNLR and IFNAR, Paneth cell numbers and lysozyme staining were restored in
270 *Atg16l1*$^{\Delta IEC}$*;Ripk3*$^{-/-}$ mice (Fig. 4C-E). These results show that RIPK3 is necessary for
271 susceptibility of *Atg16l1*$^{\Delta IEC}$ mice to MNV.

272

273 *Human organoids are susceptible to cell death induced by antiviral factors.*

274 The combination of TNF and IFNs is toxic to colonic organoids derived from humans,
275 although the concentration of cytokines necessary for cell death is high (Jang et al., 2024). Based
276 on our data with mouse organoids, we hypothesized that human small intestinal organoids will be
277 sensitive to TNF + IFN treatment, especially in the presence of the *ATG16L1* risk allele. To test
278 this hypothesis, we utilized organoids that we previously generated from endoscopic biopsy
279 specimens that were genotyped for the *ATG16L1*^{T300A} variant (Sup Table 1) (Matsuzawa-Ishimoto
280 et al., 2020). As in the mouse model, the combination of TNF + IFN-λ2 induced cell death in
281 human organoids, which was exacerbated in those derived from individuals homozygous for
282 *ATG16L1*^{T300A} (Fig. 5A-C).

283 TNF and IFNs are produced in response to most viral infections. We previously showed
284 that SARS-CoV-2 infected mice display a reduction in Paneth cell numbers and abnormal
285 lysozyme staining, reminiscent of *Atg16l1* mutant mice infected with MNV (Bernard-Raichon et
286 al., 2022). We did not detect replication competent SARS-CoV-2 particles in the gut of these mice,
287 raising the possibility that circulating antiviral cytokines can mediate long-range cytotoxic effects
288 on IECs in situations in which they reach high levels, such as observed in severe COVID (Araujo
289 et al., 2025; Ghaffarpour et al., 2025). Indeed, gastrointestinal symptoms are common in patients
290 with COVID-19 and many hospitalized patients display blood stream infections (BSI) caused by
291 microbes originating from the gut, suggesting intestinal barrier defects (Bernard-Raichon et al.,
292 2022). To test whether soluble immune mediators associated with severe COVID-19 are cytotoxic

293 to human IECs, we incubated the above organoids with serum samples pooled from hospitalized
294 patients during the height of the pandemic when individuals were screened for SARS-CoV-2
295 infection. These samples were compared with serum from healthy volunteers and hospitalized
296 individuals who were COVID-negative but BSI-positive. Compared with serum from healthy
297 volunteers, addition of serum from patients with severe COVID led to increased loss of viability,
298 which was worse in organoids homozygous for *ATG16L1*^{T300A} (Fig. 5D-F). Serum from BSI-
299 positive control also worsened organoid death but not as severely as the COVID-positive samples
300 (Fig. 5 D-F). Therefore, circulating factors associated with severe COVID-19 display cytotoxicity
301 to IECs, and the *ATG16L1* risk variant further sensitizes cells to this activity.

302

303 **Discussion**

304 Our study demonstrates that type I and III IFNs are central mediators of intestinal epithelial
305 damage following viral infection in the context of ATG16L1 deficiency. Antiviral IFNs and ISG
306 expression have been observed in IBD patients but their contribution to the pathology is
307 incompletely understood (Gunther et al., 2019; Mavragani et al., 2020; Ostvik et al., 2020;
308 Veyssiere et al., 2025). We show that IFN signaling in IECs drives epithelial cell death and disease
309 exacerbation in MNV-infected *Atg16l1*$^{\Delta IEC}$ mice, while organoid models reveal a synergistic
310 cytotoxicity between IFNs and TNF associated with necroptosis signaling. Notably, deletion of
311 IFN receptors rescued overall survival but had partial effects on Paneth cells. This may reflect a
312 confounding role for IFNs in controlling the virus, or alternatively, redundancy with other cytokines
313 such as IFN-γ, which is known to be upregulated during MNV infection and can also trigger Paneth
314 cell dysfunction (Farin et al., 2014; Matsuzawa-Ishimoto et al., 2022; Tomov et al., 2017). IFN-γ
315 and type I/III IFNs display redundancy in a model of chronic murine astrovirus infection (Herrmann
316 et al., 2025). Also, the role of IFNAR was unexpected given the dominance of IFNLR signaling in
317 IECs and may reflect selective functions in a subset of IECs or specifically in the *Atg16l1* mutant

318 setting. Future studies should explore whether each IFN has a distinct IEC target and timing of
319 activity that controls their cytotoxic effects.

320 These findings strengthen the link between infectious agents such as noroviruses and CD
321 (Axelrad et al., 2023; Axelrad et al., 2019; Cadwell & Loke, 2025). Although noroviruses are
322 associated with CD in some patients, they most often cause self-resolving gastroenteritis and are
323 detected in many asymptomatic individuals, suggesting that as in our mouse model, the
324 consequences of their presence depend on host factors and may be immune mediated (Bernard-
325 Raichon & Cadwell, 2023; Lindesmith et al., 2008). A recent study showed that Epstein-Bar virus
326 (EBV) infection precedes CD (Nandy et al., 2025). Thus, triggers of intestinal inflammation are
327 unlikely to be exclusive to noroviruses but there may be some specificity. Although many types of
328 gut microbes including commensal bacteria evoke TNF and IFNs, our finding that serum from
329 patients with severe COVID-19 displays higher toxicity to organoids compared with serum from
330 patients with non-viral BSIs raises the possibility that certain types of infections are more likely to
331 trigger responses that cause IEC death. These observations also raise the intriguing possibility
332 that viral sequelae and chronic diseases like IBD share underlying mechanisms that include IEC
333 death. However, we acknowledge that our experimental system does not allow for such
334 comparisons, and that IBD is much more complex with a prolonged disease development and
335 cycles of healing and recurrence.

336 Therapeutically targeting signaling molecules upstream of cell death may offer a strategy
337 to protect the epithelium in at-risk individuals. Although RIPK3 deletion ameliorated disease in
338 *Atg16l1*$^{\Delta IEC}$ mice *in vivo*, RIPK1 inhibition may provide broader protection by blocking multiple
339 death pathways. Crosstalk between necroptosis, apoptosis, and pyroptosis and their co-
340 occurance (Araujo et al., 2021; Malireddi & Kanneganti, 2025; Newton et al., 2014) may be
341 especially relevant to organoids that harbor multiple IEC types. Our time course experiments
342 show that necroptosis inhibition delays but does not completely prevent loss of viability in

343 organoids. The partial rescue of viability is reminiscent of findings showing that deleting *Tnfaip3*
344 and *Tnip1* (genes that are also linked to IBD and autoimmunity) sensitizes to TNF toxicity in the
345 presence of microbial and viral ligands (Rusu et al., 2022; Su et al., 2019). Interventions that can
346 be personalized to restore function of a cell type that is specifically affected in a given susceptible
347 host, such as Paneth cells in the ATG161 deficient background, may be ideal. In this sense, our
348 observation that RIPK3 deletion better restores Paneth cells compared with IFN receptor deletion
349 supports targeting nodes at the intersection of multiple cytokine signaling pathways. Indeed,
350 clinically used JAK inhibitors effectively protect patient-derived colonic organoids from cytokine
351 cocktails (Jang et al., 2024).

352 In summary, this work positions IFNs as key players in virally triggered intestinal pathology
353 associated with TNF toxicity, particularly in the setting of ATG16L1 deficiency. It underscores the
354 need to consider synergistic cytokine responses in the management of CD and other barrier-
355 associated disorders.

356

357

358

359 **Materials and Methods**

360 *Mice*

361 Age- and gender-matched 8–12-week-old mice on the C57BL/6J (B6) background were used.
362 *Atg16l1*$^{f/f}$;VillinCre (*Atg16l1*$^{\Delta IEC}$) mice were provided by S. Virgin (Washington University School
363 of Medicine, St. Louis, MO) and crossed to *Ifnar1*$^{f/f}$ (Jax, 028256) and *Ifnlr1*$^{f/f}$ mice (provided by S.
364 Virgin) to obtain *Atg16l1;Ifnar*$^{\Delta IEC}$ and *Atg16l1;Ifnlr1*$^{\Delta IEC}$ mice, respectively. To generate littermate
365 VillinCre-negative and *Atg16l1*$^{\Delta IEC}$ controls, mice were bred heterozygous for either the *Ifnar*^{f} or

366 *Ifnlr*^{f} genes and crossed VillinCre-positive with VillinCre-negative. Ifnar1$^{\Delta IEC}$ and *Ifnlr*$^{\Delta IEC}$ mice were
367 bred separately by crossing VillinCre-positive with VillinCre-negative mice. *Atg16l1;Ifnlr;Ifnar*$^{\Delta IEC}$
368 mice were obtained by crossing *Atg16l1;Ifnar1*$^{\Delta IEC}$ and *Atg16l1;Ifnlr*$^{\Delta IEC}$ mice. WT mice are a pool
369 of VillinCre-negative mice from different crosses. *Rip3*$^{-/-}$ mice were provided by G. Miller (NYU
370 School of Medicine, New York, NY). *Mlkl*$^{-/-}$ mice were provided by J. Murphy (WEHI, Parkville,
371 Australia). All animal studies were performed according to approved protocols by the New York
372 University School of Medicine Institutional Animal Care and Use Committees.

373 *MNV-triggered disease model*

374 MNV.CR6 stock was prepared as previously described (Strong et al., 2012). In brief, supernatant
375 from 293T cells transfected with a plasmid containing the viral genome was applied to RAW264.7
376 cells to amplify virus production, and virions were concentrated by ultracentrifugation and
377 resuspended in endotoxin-free PBS. Concentration of stock was determined by plaque assay as
378 previously described with few modifications (Gonzalez-Hernandez et al., 2012). Diluted stock was
379 incubated on confluent RAW264.7 cells for 1h after what cells were overlayed with 10g/L
380 methylcellulose media (Sigma-Aldrich). Cells were incubated at 37°C for 72 h and stained with
381 1g/L crystal violet solution. Mice were infected orally with 3×10^6 PFUs resuspended in PBS. Viral
382 burden in stool at day 10 post infection was determined by plaque assay as for the stock. On day
383 10 post-infection, mice were administered 5% DSS (TdB Consultancy) in their drinking water for
384 6 d after which it was replaced by regular drinking water. *Ripk3*$^{-/-}$ mice showed increased lethality
385 when given 5% DSS. When these mice were used, 3% DSS was used instead of 5% as indicated
386 in the figure legend. Clinical disease score and mouse weight were assessed daily. Disease score
387 was quantified on the basis of five parameters as described previously, including diarrhea (0–2),
388 hunched posture (0–2), fur ruffling (0 or 1), mobility (0–2), and blood stool (0 or 1), in which 8 was
389 the maximum score for the pathology (Matsuzawa-Ishimoto et al., 2017). For survival
390 experiments, mice were euthanized if they reached the humane end point. In other experiments,

391 mice were sacrificed before receiving DSS or after receiving 5 days of DSS for analysis (which
392 occurred before clinical disease signs).

393 *Intestinal organoid culture*

394 Murine small intestinal crypts were isolated and cultured as described previously using ENR
395 media composed of DMEM/F-12 (ThermoFisher) in the presence of 100IU Penicillin and 100
396 µg/ml Streptomycin (Corning), 125 µg/ml Gentamicin (ThermoFisher), 2 mML-Glutamine
397 (Corgning), 20 ng/ml mEGF (PeproTech), 100 ng/ml mNoggin (R&D systems), and 500 ng/ml
398 mR-Spondin 1 (R&D systems) (Matsuzawa-Ishimoto et al., 2017). Human organoids were
399 generated during previous studies and frozen (Jang et al., 2022; Matsuzawa-Ishimoto et al.,
400 2020). For this study, they were thawn and cultured in Human IntestiCult Organoid Growth
401 Medium (Stemcell Technologies). For viability assays, crypts were embedded at 50 crypts /10 µl
402 Matrigel (Stemcell Technologies) and cultured in triplicate for 3 days in 96-well culture plates. The
403 assay was performed in ENR medium for mouse organoids and in differentiation medium for
404 human organoids. Differentiation medium was composed of DMEM/F-12 containing 100ng/mL
405 rhIGF-1 (Biolegend), 50ng/mL hFGF-basic (PeproTech), 1µg/mL rhR-Spondin 1 (R&D systems),
406 100ng/mL rmWnt-3A (R&D systems), 100ng/mL rmNoggin (R&D systems), 10mM Nicotinamide
407 (Millipore), 10 nM [Leu15]- Gastrin 1 human (Sigma-Aldrich), 500nM A 83-01 (TOCRIS), 1X B-27
408 supplement (ThermoFisher) as in (Fujii et al., 2018; Matsuzawa-Ishimoto et al., 2022). Murine
409 organoids were treated with 20 ng/ml mTNFα (Peprotech) and indicated concentrations of mIFNβ
410 (PBL assay science) and mIFNλ2 (Peprotech). In some experiments, organoids were pre-treated
411 with 100nM Ruxolitinib, 10µM Q-VD-OPh (Millipore Sigma), 10 µM Nec-1s (Biovision), 20 µg/ml
412 anti-TNFα antibody (XT3.11, BioXcell) and 20 µg/ml Rat IgG1 isotype control (HRPN, BioXcell).
413 Human organoids were treated with 50 ng/mL hTNFα (Peprotech), 100 ng/mL hIFNλ2 (R&D
414 systems). In another experiment, half of the DMEM/F-12 in the differentiation medium was

415 replaced by human serum (growth factors were maintained at same concentrations). Serum from
416 healthy donors from the United States was purchased from SeraCare. The serum from patients
417 with BSI and SARS-CoV-2 infection was collected at the NYU Langone hospital in 2020 and also
418 used for a previous study (Table S3) (Lubkin et al., 2024). This experiment was performed in a
419 BSL2+ cell culture room to confine infectious agents. Percent viable organoids was determined
420 based on morphology by daily quantification as before (Matsuzawa-Ishimoto et al., 2017). Dead
421 organoids were also marked by staining with 100 µg/ml PI (Sigma-Aldrich) and 100 µg/ml Hoechst
422 33342 (Invitrogen) to confirm phenotypes.

423 *Quantitative qPCR*

424 RNA was extracted from organoids and intestinal tissue using the RNeasy mini kit (Qiagen). DNA
425 was removed using the RNA-free DNase set (Qiagen). cDNA was synthesized using the High-
426 Capacity cDNA reverse transcription kit (Thermo Fisher) according to the manufacturer's protocol.
427 Quantitative PCR was performed on a Roche 480 II LightCycler using SYBR Green I Master mix
428 (Roche). Gene expression was normalized to either *Gapdh* (organoids) or *β-actin* (tissue). All
429 primers are listed in Table S2.

430 *Immunoblotting*

431 600 small intestinal organoids were seeded in 24 well plates and cultured for 3 days in ENR
432 before cytokine stimulation with 20 ng/ml mTNFα in the presence of either 100 U/ml IFNβ or 1
433 ng/ml IFNλ2 for 2-24h. Organoids were incubated in lysis buffer (20 mM Tris-HCl, pH 7.4, 150
434 mM NaCl, 1% Triton X-100, 10% glycerol) containing Halt protease and phosphatase inhibitor
435 cocktail (Thermo Fisher Scientific) and run on a 4%–12% Bis-Tris Plus Gel (Invitrogen) as before
436 (Matsuzawa-Ishimoto et al., 2022). The following antibodies were used for immunoblotting
437 studies: anti–β-actin (AC-15; Sigma-Aldrich), anti–Phospho-MLKL (Ser345) and anti-MLKL (Cell

438 Signaling), anti-RIP3 (phospho S232; Abcam), anti-RIP3 (AHP1797; AbD Serotec), and anti-
439 Atg16L (Sigma-Aldrich). Secondary antibodies IRDye 680RD goat anti–rabbit IgG (925-68071)
440 and IRDye 800CW goat anti–mouse IgG (925-32210) were purchased from LI-COR.

441 *Histology and Immunohistochemistry*

442 Quantification of all microscopy data were performed blind. Intestinal sections were prepared and
443 stained as previously described (Matsuzawa-Ishimoto et al., 2022). TUNEL staining was
444 performed using the In situ Cell Death Detection POD kit (Roche Diagnostics) on the Discovery
445 XT according to the manufacturer's protocol. Lysozyme staining was performed using anti-
446 lysozyme (ab108508, Abcam) and DAPI immunostaining. All slides were analyzed using a Zeiss
447 AxioObserver.Z1 with Axiocam 503 Mono operated with Zen Blue software. Images were
448 processed and quantified using QuPath (for HE and TUNEL staining) or ImageJ (for anti-lysozyme
449 staining). At least 100 villi or crypts per mouse were quantified. Abnormal Paneth cells were
450 defined as Paneth cells showing disordered, depleted and/or diffuse lysozyme staining as in
451 (Bernard-Raichon et al., 2022; Matsuzawa-Ishimoto et al., 2022) and adapted from (Cadwell et
452 al., 2010).

453 *Statistical analysis*

454 GraphPad Prism version 10 was used for statistical analysis unless otherwise specified. *In-vivo*
455 model: Survival data were analyzed by Kaplan-Meier with Log-rank test followed by Holm Sidak's
456 multiple comparison test (Figure 1A). For other parameters measured on mice in Figure 1 and 4,
457 ordinary or lognormal ordinary (PFU, Figure 1D) one-way ANOVA and Turkey's multiple
458 comparison was used when data followed a normal distribution or a Kruskal-Wallis test followed
459 by Dunn's multiple comparison test when they did not (disease score, Figure 1B). For histological
460 measurements, the effect of mouse genotype was determined on R using individual

461 measurements (e.g. length of 50 villus per mouse) while adjusting for batch effect caused by
462 individual mouse and experiments. ANOVA type III followed by Tukey's multiple comparison
463 Generalized Linear Mixed Model (GLMM) was used for Paneth cell counts. A beta-binomial
464 analysis followed by Tukey's multiple comparison was used for Paneth cell abnormality. Negative
465 Binomial GLMM was used to compare the number of TUNEL+ cells per crypt.

466 *Murine organoids:* In Figure 2 and 3, in each experiment, organoids derived from a single mouse
467 per genotype were stimulated with different cytokines and inhibitors (experiments were then
468 repeated in independent experiments using organoids derived from different mice). Ordinary one-
469 way ANOVA were used to compare the effect of the treatment within a genotype, two-way ANOVA
470 were used when comparing the effect of the treatment and of the genotypes, followed by Sidak's
471 multiple comparison test. Comparison of area under the curve was performed to compare time-
472 course curves.

473 *Human organoids:* In Figure 5A-C, several experiments were performed to study the response of
474 each organoid donor to cytokine stimulation. The average of viability observed for each
475 stimulation in technical triplicates obtained from 2-5 experiments were calculated for each donor.
476 In Figure 5D-F, given the limited quantity of plasma available, the experiment was performed only
477 once on organoids from 3 donors per group (with technical triplicates). In both cases, an ANOVA
478 followed by Sidak's multiple comparison test was used to compare the effect of the stimulation on
479 organoid viability depending on the genotype.

480 **Acknowledgements**

481 We thank the NYU Langone's Experimental Pathology Research Laboratory
482 (RRID:SCR_017928) and the NYU Langone's Microscopy Laboratory (RRID: SCR_017934),
483 supported in part by NYU Langone Health's Laura and Isaac Perlmutter Cancer Center Support

484 (grant P30CA016087), for the use of their instruments and technical assistance. We thank the
485 following University of Pennsylvania core facilities for their expert technical support: the Cell and
486 Developmental Biology (CDB) Microscopy Core (RRID SCR_022373) as well as the Molecular
487 Pathology & Imaging Core (MPIC) (RRID: SCR_022420) and Genetically Engineered Mouse
488 Core supported by the UPENN Digestive and Liver Center (P30DK050306). We also thank M. B.
489 da Silva, Y. Shono and M. R. M. van den Brink for their support with TUNEL staining. We thank
490 Filipe De Vadder for his kind help with statistical analyses. This research was funded in part by
491 NIH grants DK093668 (K.C.), AI121244 (K.C.), AI140754 (K.C.), AI179896 (K.C.), and DK050306
492 (K.C.); Shanahan Family Fund for Inflammatory Bowel Disease Research (K.C.); pilot grant from
493 King Center for Lynch Syndrome (K.C.); pilot grant from Abramson Cancer Center (K.C.); and an
494 industry partnership with AbbVie Inc. (K.C.).

495 **Declaration of interests**

496 K.C. has received research funding from Pfizer, Takeda, Pacific Biosciences, Genentech and
497 Abbvie. K.C. has consulted for or received an honorarium for speaking engagement from
498 Puretech Health, Genentech, Moderna, Gentibio, Pioneering Medicines, and Abbvie. K.C. is an
499 inventor on US patent 10,722,600 and provisional patent 63/157,225. J.A. has received research
500 grants from BioFire Diagnostics, Genentech, Takeda, and Johnson & Johnson; consultancy fees,
501 honorarium, or advisory board fees from Abbvie, Abviax, Adiso, BioFire Diagnostics, Biomerieux,
502 Bristol-Myers Squibb, Celltrion, Ferring, Fresenius, Johnson & Johnson, Johnson & Johnson,
503 Merck, Pfizer, Sanofi, Takeda, and Vedanta. V.J.T. is an inventor on patents and patent
504 applications filed by New York University, which are currently under commercial license to
505 Janssen Biotech Inc. Janssen Biotech Inc. provides research funding and other payments
506 associated with the licensing agreement.

507

508

509 **Author contributions**

510 LBR, JAN, YMI and KC designed the study. LBR, JAN and YMI performed most of the
511 experiments with assistance from KK, TH, and DM and BMM. YMI and JA provided the human
512 organoids lines. AL, AD and VJT provided the human serum samples. LBR, JAN and KC drafted
513 the manuscript. All authors contributed to refinement of the study protocol and approved the final
514 manuscript.

515

516 **References**

517 Abt, M. C., Buffie, C. G., Susac, B., Becattini, S., Carter, R. A., Leiner, I., Keith, J. W., Artis, D.,
518 Osborne, L. C., & Pamer, E. G. (2016). TLR-7 activation enhances IL-22-mediated
519 colonization resistance against vancomycin-resistant enterococcus. *Sci Transl Med*,
520 *8*(327), 327ra325. https://doi.org/10.1126/scitranslmed.aad6663
521 Aden, K., Tran, F., Ito, G., Sheibani-Tezerji, R., Lipinski, S., Kuiper, J. W., Tschurtschenthaler,
522 M., Saveljeva, S., Bhattacharyya, J., Hasler, R., Bartsch, K., Luzius, A., Jentzsch, M., Falk-
523 Paulsen, M., Stengel, S. T., Welz, L., Schwarzer, R., Rabe, B., Barchet, W.,…Rosenstiel,
524 P. (2018). ATG16L1 orchestrates interleukin-22 signaling in the intestinal epithelium via
525 cGAS-STING. *J Exp Med*, *215*(11), 2868-2886. https://doi.org/10.1084/jem.20171029
526 Adolph, T. E., Tomczak, M. F., Niederreiter, L., Ko, H. J., Bock, J., Martinez-Naves, E., Glickman,
527 J. N., Tschurtschenthaler, M., Hartwig, J., Hosomi, S., Flak, M. B., Cusick, J. L., Kohno,
528 K., Iwawaki, T., Billmann-Born, S., Raine, T., Bharti, R., Lucius, R., Kweon, M.
529 N.,…Blumberg, R. S. (2013). Paneth cells as a site of origin for intestinal inflammation.
530 *Nature*, *503*(7475), 272-276. https://doi.org/10.1038/nature12599
531 Aktepe, T. E., Deerain, J. M., Hyde, J. L., Fritzlar, S., Mead, E. M., Carrera Montoya, J., Hachani,
532 A., Pearson, J. S., White, P. A., & Mackenzie, J. M. (2024). Norovirus-mediated translation
533 repression promotes macrophage cell death. *PLoS Pathog*, *20*(9), e1012480.
534 https://doi.org/10.1371/journal.ppat.1012480
535 Araujo, A., Safronova, A., Burger, E., Lopez-Yglesias, A., Giri, S., Camanzo, E. T., Martin, A. T.,
536 Grivennikov, S., & Yarovinsky, F. (2021). IFN-gamma mediates Paneth cell death via
537 suppression of mTOR. *Elife*, *10*. https://doi.org/10.7554/eLife.60478
538 Araujo, R., Von Rekowski, C. P., Fonseca, T. A. H., Calado, C. R. C., Ramalhete, L., & Bento, L.
539 (2025). Multiplex Targeted Proteomic Analysis of Cytokine Ratios for ICU Mortality in
540 Severe COVID-19. *Proteomes*, *13*(3). https://doi.org/10.3390/proteomes13030035
541 Ardanuy, J., Scanlon, K., Skerry, C., Fuchs, S. Y., & Carbonetti, N. H. (2020). Age-Dependent
542 Effects of Type I and Type III IFNs in the Pathogenesis of Bordetella pertussis Infection
543 and Disease. *J Immunol*, *204*(8), 2192-2202. https://doi.org/10.4049/jimmunol.1900912
544 Asano, J., Sato, T., Ichinose, S., Kajita, M., Onai, N., Shimizu, S., & Ohteki, T. (2017). Intrinsic
545 Autophagy Is Required for the Maintenance of Intestinal Stem Cells and for Irradiation-
546 Induced Intestinal Regeneration. *Cell Rep*, *20*(5), 1050-1060.
547 https://doi.org/10.1016/j.celrep.2017.07.019

548 Axelrad, J. E., Chen, Z., Devlin, J., Ruggles, K. V., & Cadwell, K. (2023). Pathogen-Specific
549 Alterations in the Gut Microbiota Predict Outcomes in Flare of Inflammatory Bowel
550 Disease Complicated by Gastrointestinal Infection. *Clin Transl Gastroenterol*, *14*(2),
551 e00550. https://doi.org/10.14309/ctg.0000000000000550
552 Axelrad, J. E., Olen, O., Askling, J., Lebwohl, B., Khalili, H., Sachs, M. C., & Ludvigsson, J. F.
553 (2019). Gastrointestinal Infection Increases Odds of Inflammatory Bowel Disease in a
554 Nationwide Case-Control Study. *Clin Gastroenterol Hepatol*, *17*(7), 1311-1322 e1317.
555 https://doi.org/10.1016/j.cgh.2018.09.034
556 Baldridge, M. T., Lee, S., Brown, J. J., McAllister, N., Urbanek, K., Dermody, T. S., Nice, T. J., &
557 Virgin, H. W. (2017). Expression of Ifnlr1 on Intestinal Epithelial Cells Is Critical to the
558 Antiviral Effects of Interferon Lambda against Norovirus and Reovirus. *J Virol*, *91*(7).
559 https://doi.org/10.1128/JVI.02079-16
560 Bel, S., Pendse, M., Wang, Y., Li, Y., Ruhn, K. A., Hassell, B., Leal, T., Winter, S. E., Xavier, R.
561 J., & Hooper, L. V. (2017). Paneth cells secrete lysozyme via secretory autophagy during
562 bacterial infection of the intestine. *Science*, *357*(6355), 1047-1052.
563 https://doi.org/10.1126/science.aal4677
564 Benjamin, J. L., Sumpter, R., Jr., Levine, B., & Hooper, L. V. (2013). Intestinal epithelial autophagy
565 is essential for host defense against invasive bacteria. *Cell Host Microbe*, *13*(6), 723-734.
566 https://doi.org/10.1016/j.chom.2013.05.004
567 Bernard-Raichon, L., & Cadwell, K. (2023). Immunomodulation by Enteric Viruses. *Annu Rev*
568 *Virol*, *10*(1), 477-502. https://doi.org/10.1146/annurev-virology-111821-112317
569 Bernard-Raichon, L., Venzon, M., Klein, J., Axelrad, J. E., Zhang, C., Sullivan, A. P., Hussey, G.
570 A., Casanovas-Massana, A., Noval, M. G., Valero-Jimenez, A. M., Gago, J., Putzel, G.,
571 Pironti, A., Wilder, E., Yale, I. R. T., Thorpe, L. E., Littman, D. R., Dittmann, M., Stapleford,
572 K. A.,…Schluter, J. (2022). Gut microbiome dysbiosis in antibiotic-treated COVID-19
573 patients is associated with microbial translocation and bacteremia. *Nat Commun*, *13*(1),
574 5926. https://doi.org/10.1038/s41467-022-33395-6
575 Bok, K., Prikhodko, V. G., Green, K. Y., & Sosnovtsev, S. V. (2009). Apoptosis in murine
576 norovirus-infected RAW264.7 cells is associated with downregulation of survivin. *J Virol*,
577 *83*(8), 3647-3656. https://doi.org/10.1128/JVI.02028-08
578 Burger, E., Araujo, A., Lopez-Yglesias, A., Rajala, M. W., Geng, L., Levine, B., Hooper, L. V.,
579 Burstein, E., & Yarovinsky, F. (2018). Loss of Paneth Cell Autophagy Causes Acute
580 Susceptibility to Toxoplasma gondii-Mediated Inflammation. *Cell Host Microbe*, *23*(2),
581 177-190 e174. https://doi.org/10.1016/j.chom.2018.01.001
582 Cadwell, K., Liu, J. Y., Brown, S. L., Miyoshi, H., Loh, J., Lennerz, J. K., Kishi, C., Kc, W., Carrero,
583 J. A., Hunt, S., Stone, C. D., Brunt, E. M., Xavier, R. J., Sleckman, B. P., Li, E., Mizushima,
584 N., Stappenbeck, T. S., & Virgin, H. W. t. (2008). A key role for autophagy and the
585 autophagy gene Atg16l1 in mouse and human intestinal Paneth cells. *Nature*, *456*(7219),
586 259-263. https://doi.org/10.1038/nature07416
587 Cadwell, K., & Loke, P. (2025). Gene-environment interactions shape the host-microbial interface
588 in inflammatory bowel disease. *Nat Immunol*, *26*(7), 1023-1035.
589 https://doi.org/10.1038/s41590-025-02197-5
590 Cadwell, K., Patel, K. K., Maloney, N. S., Liu, T. C., Ng, A. C., Storer, C. E., Head, R. D., Xavier,
591 R., Stappenbeck, T. S., & Virgin, H. W. (2010). Virus-plus-susceptibility gene interaction
592 determines Crohn's disease gene Atg16L1 phenotypes in intestine. *Cell*, *141*(7), 1135-
593 1145. https://doi.org/10.1016/j.cell.2010.05.009
594 Churchill, M. J., Mitchell, P. S., & Rauch, I. (2022). Epithelial Pyroptosis in Host Defense. *J Mol*
595 *Biol*, *434*(4), 167278. https://doi.org/10.1016/j.jmb.2021.167278
596 Conway, K. L., Kuballa, P., Song, J. H., Patel, K. K., Castoreno, A. B., Yilmaz, O. H., Jijon, H. B.,
597 Zhang, M., Aldrich, L. N., Villablanca, E. J., Peloquin, J. M., Goel, G., Lee, I. A., Mizoguchi,
598 E., Shi, H. N., Bhan, A. K., Shaw, S. Y., Schreiber, S. L., Virgin, H. W.,…Xavier, R. J.

599 (2013). Atg16l1 is required for autophagy in intestinal epithelial cells and protection of mice
600 from Salmonella infection. *Gastroenterology*, *145*(6), 1347-1357.
601 https://doi.org/10.1053/j.gastro.2013.08.035
602 Dannappel, M., Vlantis, K., Kumari, S., Polykratis, A., Kim, C., Wachsmuth, L., Eftychi, C., Lin, J.,
603 Corona, T., Hermance, N., Zelic, M., Kirsch, P., Basic, M., Bleich, A., Kelliher, M., &
604 Pasparakis, M. (2014). RIPK1 maintains epithelial homeostasis by inhibiting apoptosis and
605 necroptosis. *Nature*, *513*(7516), 90-94. https://doi.org/10.1038/nature13608
606 Deerain, J. M., Aktepe, T. E., Trenerry, A. M., Ebert, G., Hyde, J. L., Charry, K., Edgington-
607 Mitchell, L., Xu, B., Ambrose, R. L., Sarvestani, S. T., Lawlor, K. E., Pearson, J. S., White,
608 P. A., & Mackenzie, J. M. (2024). Murine norovirus infection of macrophages induces
609 intrinsic apoptosis as the major form of programmed cell death. *Virology*, *589*, 109921.
610 https://doi.org/10.1016/j.virol.2023.109921
611 Farin, H. F., Karthaus, W. R., Kujala, P., Rakhshandehroo, M., Schwank, G., Vries, R. G.,
612 Kalkhoven, E., Nieuwenhuis, E. E., & Clevers, H. (2014). Paneth cell extrusion and release
613 of antimicrobial products is directly controlled by immune cell-derived IFN-gamma. *J Exp*
614 *Med*, *211*(7), 1393-1405. https://doi.org/10.1084/jem.20130753
615 Foerster, E. G., Tsang, D. K. L., Goyal, S., Robertson, S. J., Robert, L. M., Maughan, H., Streutker,
616 C. J., Girardin, S. E., & Philpott, D. J. (2023). ATG16L1 protects from interferon-gamma-
617 induced cell death in the small intestinal crypt. *Mucosal Immunol*, *16*(2), 135-152.
618 https://doi.org/10.1016/j.mucimm.2023.02.001
619 Fujii, M., Matano, M., Toshimitsu, K., Takano, A., Mikami, Y., Nishikori, S., Sugimoto, S., & Sato,
620 T. (2018). Human Intestinal Organoids Maintain Self-Renewal Capacity and Cellular
621 Diversity in Niche-Inspired Culture Condition. *Cell Stem Cell*, *23*(6), 787-793 e786.
622 https://doi.org/10.1016/j.stem.2018.11.016
623 Ghaffarpour, S., Ghazanfari, T., Ardestani, S. K., Naghizadeh, M. M., Vaez Mahdavi, M. R.,
624 Salehi, M., Majd, A. M. M., Rashidi, A., Chenary, M. R., Mostafazadeh, A., Rezaei, A.,
625 Khodadadi, A., Iranparast, S., & Khazaei, H. A. (2025). Cytokine profiles dynamics in
626 COVID-19 patients: a longitudinal analysis of disease severity and outcomes. *Sci Rep*,
627 *15*(1), 14209. https://doi.org/10.1038/s41598-025-98505-y
628 Gonzalez-Hernandez, M. B., Bragazzi Cunha, J., & Wobus, C. E. (2012). Plaque assay for murine
629 norovirus. *J Vis Exp*(66), e4297. https://doi.org/10.3791/4297
630 Graziano, V. R., Alfajaro, M. M., Schmitz, C. O., Filler, R. B., Strine, M. S., Wei, J., Hsieh, L. L.,
631 Baldridge, M. T., Nice, T. J., Lee, S., Orchard, R. C., & Wilen, C. B. (2021). CD300lf
632 Conditional Knockout Mouse Reveals Strain-Specific Cellular Tropism of Murine
633 Norovirus. *J Virol*, *95*(3). https://doi.org/10.1128/JVI.01652-20
634 Gunther, C., Ruder, B., Stolzer, I., Dorner, H., He, G. W., Chiriac, M. T., Aden, K., Strigli, A., Bittel,
635 M., Zeissig, S., Rosenstiel, P., Atreya, R., Neurath, M. F., Wirtz, S., & Becker, C. (2019).
636 Interferon Lambda Promotes Paneth Cell Death Via STAT1 Signaling in Mice and Is
637 Increased in Inflamed Ileal Tissues of Patients With Crohn's Disease. *Gastroenterology*,
638 *157*(5), 1310-1322 e1313. https://doi.org/10.1053/j.gastro.2019.07.031
639 Herrmann, C., Zaldana, K., Lustig, A. M., Bee, G. C. W., Agostino, E. L., Koralov, S. B., & Cadwell,
640 K. (2025). Environmental stress drives clearance of a persistent enteric virus in mice. *Nat*
641 *Microbiol*, *10*(8), 1975-1988. https://doi.org/10.1038/s41564-025-02046-z
642 Ingle, H., Peterson, S. T., & Baldridge, M. T. (2018). Distinct Effects of Type I and III Interferons
643 on Enteric Viruses. *Viruses*, *10*(1). https://doi.org/10.3390/v10010046
644 Jackson, D. N., Panopoulos, M., Neumann, W. L., Turner, K., Cantarel, B. L., Thompson-Snipes,
645 L., Dassopoulos, T., Feagins, L. A., Souza, R. F., Mills, J. C., Blumberg, R. S.,
646 Venuprasad, K., Thompson, W. E., & Theiss, A. L. (2020). Mitochondrial dysfunction
647 during loss of prohibitin 1 triggers Paneth cell defects and ileitis. *Gut*, *69*(11), 1928-1938.
648 https://doi.org/10.1136/gutjnl-2019-319523

649 Jang, K. K., Hudesman, D., Jones, D. R., Loke, P., Axelrad, J. E., Cadwell, K., & Tofacitinib
650 Working, G. (2024). Tofacitinib Uptake by Patient-Derived Intestinal Organoids Predicts
651 Individual Clinical Responsiveness. *Gastroenterology*, *167*(7), 1453-1456 e1455.
652 https://doi.org/10.1053/j.gastro.2024.07.035
653 Jang, K. K., Kaczmarek, M. E., Dallari, S., Chen, Y. H., Tada, T., Axelrad, J., Landau, N. R.,
654 Stapleford, K. A., & Cadwell, K. (2022). Variable susceptibility of intestinal organoid-
655 derived monolayers to SARS-CoV-2 infection. *PLoS Biol*, *20*(3), e3001592.
656 https://doi.org/10.1371/journal.pbio.3001592
657 Jena, K. K., Mambu, J., Boehmer, D., Sposito, B., Millet, V., de Sousa Casal, J., Muendlein, H. I.,
658 Spreafico, R., Fenouil, R., Spinelli, L., Wurbel, S., Riquier, C., Galland, F., Naquet, P.,
659 Chasson, L., Elkins, M., Mitsialis, V., Ketelut-Carneiro, N., Bugda Gwilt, K.,…Zanoni, I.
660 (2024). Type III interferons induce pyroptosis in gut epithelial cells and impair mucosal
661 repair. *Cell*, *187*(26), 7533-7550 e7523. https://doi.org/10.1016/j.cell.2024.10.010
662 Jung, H., Leal-Ekman, J. S., Lu, Q., & Stappenbeck, T. S. (2019). Atg14 protects the intestinal
663 epithelium from TNF-triggered villus atrophy. *Autophagy*, *15*(11), 1990-2001.
664 https://doi.org/10.1080/15548627.2019.1596495
665 Kattah, M. G., Shao, L., Rosli, Y. Y., Shimizu, H., Whang, M. I., Advincula, R., Achacoso, P.,
666 Shah, S., Duong, B. H., Onizawa, M., Tanbun, P., Malynn, B. A., & Ma, A. (2018). A20
667 and ABIN-1 synergistically preserve intestinal epithelial cell survival. *J Exp Med*, *215*(7),
668 1839-1852. https://doi.org/10.1084/jem.20180198
669 Kernbauer, E., Ding, Y., & Cadwell, K. (2014). An enteric virus can replace the beneficial function
670 of commensal bacteria. *Nature*, *516*(7529), 94-98. https://doi.org/10.1038/nature13960
671 Lee, S., Wilen, C. B., Orvedahl, A., McCune, B. T., Kim, K. W., Orchard, R. C., Peterson, S. T.,
672 Nice, T. J., Baldridge, M. T., & Virgin, H. W. (2017). Norovirus Cell Tropism Is Determined
673 by Combinatorial Action of a Viral Non-structural Protein and Host Cytokine. *Cell Host*
674 *Microbe*, *22*(4), 449-459 e444. https://doi.org/10.1016/j.chom.2017.08.021
675 Lim, J., Park, H., Heisler, J., Maculins, T., Roose-Girma, M., Xu, M., McKenzie, B., van Lookeren
676 Campagne, M., Newton, K., & Murthy, A. (2019). Autophagy regulates inflammatory
677 programmed cell death via turnover of RHIM-domain proteins. *Elife*, *8*.
678 https://doi.org/10.7554/eLife.44452
679 Lin, J. D., Feng, N., Sen, A., Balan, M., Tseng, H. C., McElrath, C., Smirnov, S. V., Peng, J.,
680 Yasukawa, L. L., Durbin, R. K., Durbin, J. E., Greenberg, H. B., & Kotenko, S. V. (2016).
681 Distinct Roles of Type I and Type III Interferons in Intestinal Immunity to Homologous and
682 Heterologous Rotavirus Infections. *PLoS Pathog*, *12*(4), e1005600.
683 https://doi.org/10.1371/journal.ppat.1005600
684 Lindesmith, L. C., Donaldson, E. F., Lobue, A. D., Cannon, J. L., Zheng, D. P., Vinje, J., & Baric,
685 R. S. (2008). Mechanisms of GII.4 norovirus persistence in human populations. *PLoS*
686 *Med*, *5*(2), e31. https://doi.org/10.1371/journal.pmed.0050031
687 Lubkin, A., Bernard-Raichon, L., DuMont, A. L., Valero Jimenez, A. M., Putzel, G. G., Gago, J.,
688 Zwack, E. E., Olusanya, O., Boguslawski, K. M., Dallari, S., Dyzenhaus, S., Herrmann, C.,
689 Ilmain, J. K., Isom, G. L., Pawline, M., Perault, A. I., Perelman, S., Sause, W. E., Shahi,
690 I.,…Torres, V. J. (2024). SARS-CoV-2 infection predisposes patients to coinfection with
691 Staphylococcus aureus. *mBio*, *15*(8), e0166724. https://doi.org/10.1128/mbio.01667-24
692 Mahlakoiv, T., Hernandez, P., Gronke, K., Diefenbach, A., & Staeheli, P. (2015). Leukocyte-
693 derived IFN-alpha/beta and epithelial IFN-lambda constitute a compartmentalized
694 mucosal defense system that restricts enteric virus infections. *PLoS Pathog*, *11*(4),
695 e1004782. https://doi.org/10.1371/journal.ppat.1004782
696 Malireddi, R. K. S., & Kanneganti, T. D. (2025). Three decades of caspases and RIPKs in life and
697 death. *Hum Mol Genet*, *34*(R1), R121-R136. https://doi.org/10.1093/hmg/ddaf106
698 Marchiando, A. M., Ramanan, D., Ding, Y., Gomez, L. E., Hubbard-Lucey, V. M., Maurer, K.,
699 Wang, C., Ziel, J. W., van Rooijen, N., Nunez, G., Finlay, B. B., Mysorekar, I. U., &

Cadwell, K. (2013). A deficiency in the autophagy gene Atg16L1 enhances resistance to enteric bacterial infection. *Cell Host Microbe*, *14*(2), 216-224. https://doi.org/10.1016/j.chom.2013.07.013

Martin, P. K., Marchiando, A., Xu, R., Rudensky, E., Yeung, F., Schuster, S. L., Kernbauer, E., & Cadwell, K. (2018). Autophagy proteins suppress protective type I interferon signalling in response to the murine gut microbiota. *Nat Microbiol*, *3*(10), 1131-1141. https://doi.org/10.1038/s41564-018-0229-0

Matsuzawa-Ishimoto, Y., Hine, A., Shono, Y., Rudensky, E., Lazrak, A., Yeung, F., Neil, J. A., Yao, X., Chen, Y. H., Heaney, T., Schuster, S. L., Zwack, E. E., Axelrad, J. E., Hudesman, D., Tsai, J. J., Nichols, K., Dewan, M. Z., Cammer, M., Beal, A.,…Cadwell, K. (2020). An intestinal organoid-based platform that recreates susceptibility to T-cell-mediated tissue injury. *Blood*, *135*(26), 2388-2401. https://doi.org/10.1182/blood.2019004116

Matsuzawa-Ishimoto, Y., Hwang, S., & Cadwell, K. (2018). Autophagy and Inflammation. *Annu Rev Immunol*, *36*, 73-101. https://doi.org/10.1146/annurev-immunol-042617-053253

Matsuzawa-Ishimoto, Y., Shono, Y., Gomez, L. E., Hubbard-Lucey, V. M., Cammer, M., Neil, J., Dewan, M. Z., Lieberman, S. R., Lazrak, A., Marinis, J. M., Beal, A., Harris, P. A., Bertin, J., Liu, C., Ding, Y., van den Brink, M. R. M., & Cadwell, K. (2017). Autophagy protein ATG16L1 prevents necroptosis in the intestinal epithelium. *J Exp Med*, *214*(12), 3687-3705. https://doi.org/10.1084/jem.20170558

Matsuzawa-Ishimoto, Y., Yao, X., Koide, A., Ueberheide, B. M., Axelrad, J. E., Reis, B. S., Parsa, R., Neil, J. A., Devlin, J. C., Rudensky, E., Dewan, M. Z., Cammer, M., Blumberg, R. S., Ding, Y., Ruggles, K. V., Mucida, D., Koide, S., & Cadwell, K. (2022). The gammadelta IEL effector API5 masks genetic susceptibility to Paneth cell death. *Nature*, *610*(7932), 547-554. https://doi.org/10.1038/s41586-022-05259-y

Mavragani, C. P., Nezos, A., Dovrolis, N., Andreou, N. P., Legaki, E., Sechi, L. A., Bamias, G., & Gazouli, M. (2020). Type I and II Interferon Signatures Can Predict the Response to Anti-TNF Agents in Inflammatory Bowel Disease Patients: Involvement of the Microbiota. *Inflamm Bowel Dis*, *26*(10), 1543-1553. https://doi.org/10.1093/ibd/izaa216

McElrath, C., Espinosa, V., Lin, J. D., Peng, J., Sridhar, R., Dutta, O., Tseng, H. C., Smirnov, S. V., Risman, H., Sandoval, M. J., Davra, V., Chang, Y. J., Pollack, B. P., Birge, R. B., Galan, M., Rivera, A., Durbin, J. E., & Kotenko, S. V. (2021). Critical role of interferons in gastrointestinal injury repair. *Nat Commun*, *12*(1), 2624. https://doi.org/10.1038/s41467-021-22928-0

Nandy, A., Petralia, F., Porter, C. K., Elledge, S., Viruses, Group, I. B. D. S., Colombel, J. F., & Snapper, S. B. (2025). Epstein-Barr Virus Exposure Precedes Crohn's Disease Development. *Gastroenterology*, *169*(1), 150-153. https://doi.org/10.1053/j.gastro.2025.01.247

Neil, J. A., Matsuzawa-Ishimoto, Y., Kernbauer-Holzl, E., Schuster, S. L., Sota, S., Venzon, M., Dallari, S., Galvao Neto, A., Hine, A., Hudesman, D., Loke, P., Nice, T. J., & Cadwell, K. (2019). IFN-I and IL-22 mediate protective effects of intestinal viral infection. *Nat Microbiol*, *4*(10), 1737-1749. https://doi.org/10.1038/s41564-019-0470-1

Newton, K., Dugger, D. L., Wickliffe, K. E., Kapoor, N., de Almagro, M. C., Vucic, D., Komuves, L., Ferrando, R. E., French, D. M., Webster, J., Roose-Girma, M., Warming, S., & Dixit, V. M. (2014). Activity of protein kinase RIPK3 determines whether cells die by necroptosis or apoptosis. *Science*, *343*(6177), 1357-1360. https://doi.org/10.1126/science.1249361

Nice, T. J., Baldridge, M. T., McCune, B. T., Norman, J. M., Lazear, H. M., Artyomov, M., Diamond, M. S., & Virgin, H. W. (2015). Interferon-lambda cures persistent murine norovirus infection in the absence of adaptive immunity. *Science*, *347*(6219), 269-273. https://doi.org/10.1126/science.1258100

Nice, T. J., Osborne, L. C., Tomov, V. T., Artis, D., Wherry, E. J., & Virgin, H. W. (2016). Type I Interferon Receptor Deficiency in Dendritic Cells Facilitates Systemic Murine Norovirus

751 Persistence Despite Enhanced Adaptive Immunity. *PLoS Pathog*, *12*(6), e1005684.
752 https://doi.org/10.1371/journal.ppat.1005684
753 Odendall, C., Dixit, E., Stavru, F., Bierne, H., Franz, K. M., Durbin, A. F., Boulant, S., Gehrke, L.,
754 Cossart, P., & Kagan, J. C. (2014). Diverse intracellular pathogens activate type III
755 interferon expression from peroxisomes. *Nat Immunol*, *15*(8), 717-726.
756 https://doi.org/10.1038/ni.2915
757 Orchard, R. C., Wilen, C. B., Doench, J. G., Baldridge, M. T., McCune, B. T., Lee, Y. C., Lee, S.,
758 Pruett-Miller, S. M., Nelson, C. A., Fremont, D. H., & Virgin, H. W. (2016). Discovery of a
759 proteinaceous cellular receptor for a norovirus. *Science*, *353*(6302), 933-936.
760 https://doi.org/10.1126/science.aaf1220
761 Ostvik, A. E., Svendsen, T. D., Granlund, A. V. B., Doseth, B., Skovdahl, H. K., Bakke, I., Thorsvik,
762 S., Afroz, W., Walaas, G. A., Mollnes, T. E., Gustafsson, B. I., Sandvik, A. K., & Bruland,
763 T. (2020). Intestinal Epithelial Cells Express Immunomodulatory ISG15 During Active
764 Ulcerative Colitis and Crohn's Disease. *J Crohns Colitis*, *14*(7), 920-934.
765 https://doi.org/10.1093/ecco-jcc/jjaa022
766 Patankar, J. V., & Becker, C. (2020). Cell death in the gut epithelium and implications for chronic
767 inflammation. *Nat Rev Gastroenterol Hepatol*, *17*(9), 543-556.
768 https://doi.org/10.1038/s41575-020-0326-4
769 Patel, K. K., Miyoshi, H., Beatty, W. L., Head, R. D., Malvin, N. P., Cadwell, K., Guan, J. L., Saitoh,
770 T., Akira, S., Seglen, P. O., Dinauer, M. C., Virgin, H. W., & Stappenbeck, T. S. (2013).
771 Autophagy proteins control goblet cell function by potentiating reactive oxygen species
772 production. *EMBO J*, *32*(24), 3130-3144. https://doi.org/10.1038/emboj.2013.233
773 Pott, J., Kabat, A. M., & Maloy, K. J. (2018). Intestinal Epithelial Cell Autophagy Is Required to
774 Protect against TNF-Induced Apoptosis during Chronic Colitis in Mice. *Cell Host Microbe*,
775 *23*(2), 191-202 e194. https://doi.org/10.1016/j.chom.2017.12.017
776 Ramanan, D., & Cadwell, K. (2016). Intrinsic Defense Mechanisms of the Intestinal Epithelium.
777 *Cell Host Microbe*, *19*(4), 434-441. https://doi.org/10.1016/j.chom.2016.03.003
778 Robinson, B. A., Van Winkle, J. A., McCune, B. T., Peters, A. M., & Nice, T. J. (2019). Caspase-
779 mediated cleavage of murine norovirus NS1/2 potentiates apoptosis and is required for
780 persistent infection of intestinal epithelial cells. *PLoS Pathog*, *15*(7), e1007940.
781 https://doi.org/10.1371/journal.ppat.1007940
782 Rocha-Pereira, J., Jacobs, S., Noppen, S., Verbeken, E., Michiels, T., & Neyts, J. (2018).
783 Interferon lambda (IFN-lambda) efficiently blocks norovirus transmission in a mouse
784 model. *Antiviral Res*, *149*, 7-15. https://doi.org/10.1016/j.antiviral.2017.10.017
785 Rusu, I., Mennillo, E., Bain, J. L., Li, Z., Sun, X., Ly, K. M., Rosli, Y. Y., Naser, M., Wang, Z.,
786 Advincula, R., Achacoso, P., Shao, L., Razani, B., Klein, O. D., Marson, A., Turnbaugh, J.
787 A., Turnbaugh, P. J., Malynn, B. A., Ma, A., & Kattah, M. G. (2022). Microbial signals,
788 MyD88, and lymphotoxin drive TNF-independent intestinal epithelial tissue damage. *J Clin*
789 *Invest*, *132*(5). https://doi.org/10.1172/JCI154993
790 Song, J., Zhang, L., Moon, S., Fang, A., Wang, G., Gheshm, N., Loeb, S. A., Cao, P., Wallace, J.
791 R., Alfajaro, M. M., Strine, M. S., Beatty, W. L., Jamieson, A. M., Orchard, R. C., Robinson,
792 B. A., Nice, T. J., Wilen, C. B., Orvedahl, A., Reese, T. A., & Lee, S. (2025). Norovirus co-
793 opts NINJ1 for selective protein secretion. *Sci Adv*, *11*(9), eadu7985.
794 https://doi.org/10.1126/sciadv.adu7985
795 Strong, D. W., Thackray, L. B., Smith, T. J., & Virgin, H. W. (2012). Protruding domain of capsid
796 protein is necessary and sufficient to determine murine norovirus replication and
797 pathogenesis in vivo. *J Virol*, *86*(6), 2950-2958. https://doi.org/10.1128/JVI.07038-11
798 Su, Z., Dziedzic, S. A., Hu, D., Barrett, V. J., Broekema, N., Li, W., Qian, L., Jia, N., Ofengeim,
799 D., Najafov, A., Zhu, H., Knipe, D. M., & Yuan, J. (2019). ABIN-1 heterozygosity sensitizes
800 to innate immune response in both RIPK1-dependent and RIPK1-independent manner.
801 *Cell Death Differ*, *26*(6), 1077-1088. https://doi.org/10.1038/s41418-018-0215-3

802 Thackray, L. B., Duan, E., Lazear, H. M., Kambal, A., Schreiber, R. D., Diamond, M. S., & Virgin,
803 H. W. (2012). Critical role for interferon regulatory factor 3 (IRF-3) and IRF-7 in type I
804 interferon-mediated control of murine norovirus replication. *J Virol*, *86*(24), 13515-13523.
805 https://doi.org/10.1128/JVI.01824-12
806 Tomov, V. T., Palko, O., Lau, C. W., Pattekar, A., Sun, Y., Tacheva, R., Bengsch, B., Manne, S.,
807 Cosma, G. L., Eisenlohr, L. C., Nice, T. J., Virgin, H. W., & Wherry, E. J. (2017).
808 Differentiation and Protective Capacity of Virus-Specific CD8(+) T Cells Suggest Murine
809 Norovirus Persistence in an Immune-Privileged Enteric Niche. *Immunity*, *47*(4), 723-738
810 e725. https://doi.org/10.1016/j.immuni.2017.09.017
811 Tschurtschenthaler, M., Adolph, T. E., Ashcroft, J. W., Niederreiter, L., Bharti, R., Saveljeva, S.,
812 Bhattacharyya, J., Flak, M. B., Shih, D. Q., Fuhler, G. M., Parkes, M., Kohno, K., Iwawaki,
813 T., Janneke van der Woude, C., Harding, H. P., Smith, A. M., Peppelenbosch, M. P.,
814 Targan, S. R., Ron, D.,…Kaser, A. (2017). Defective ATG16L1-mediated removal of
815 IRE1alpha drives Crohn's disease-like ileitis. *J Exp Med*, *214*(2), 401-422.
816 https://doi.org/10.1084/jem.20160791
817 Van Winkle, J. A., Peterson, S. T., Kennedy, E. A., Wheadon, M. J., Ingle, H., Desai, C., Rodgers,
818 R., Constant, D. A., Wright, A. P., Li, L., Artyomov, M. N., Lee, S., Baldridge, M. T., & Nice,
819 T. J. (2022). Homeostatic interferon-lambda response to bacterial microbiota stimulates
820 preemptive antiviral defense within discrete pockets of intestinal epithelium. *Elife*, *11*.
821 https://doi.org/10.7554/eLife.74072
822 Veyssiere, M., Hammoudi, N., Le Bourhis, L., Hassid, D., Bonnet, J., Tran Minh, M. L., Baudry,
823 C., Gornet, J. M., Chardiny, V., Seksik, P., Nancey, S., Carbonnel, F., Treton, X., Wils, P.,
824 Buisson, A., Boureille, A., Hebuterne, X., Serrero, M., Fumery, M.,…Allez, M. (2025).
825 Blood proteomic signatures associated with disease activity in inflammatory bowel
826 diseases. *J Crohns Colitis*, *19*(9). https://doi.org/10.1093/ecco-jcc/jjaf162
827 Wang, G., Zhang, D., Orchard, R. C., Hancks, D. C., & Reese, T. A. (2023). Norovirus MLKL-like
828 protein initiates cell death to induce viral egress. *Nature*, *616*(7955), 152-158.
829 https://doi.org/10.1038/s41586-023-05851-w
830 Wilen, C. B., Lee, S., Hsieh, L. L., Orchard, R. C., Desai, C., Hykes, B. L., Jr., McAllaster, M. R.,
831 Balce, D. R., Feehley, T., Brestoff, J. R., Hickey, C. A., Yokoyama, C. C., Wang, Y. T.,
832 MacDuff, D. A., Kreamalmayer, D., Howitt, M. R., Neil, J. A., Cadwell, K., Allen, P.
833 M.,…Virgin, H. W. (2018). Tropism for tuft cells determines immune promotion of norovirus
834 pathogenesis. *Science*, *360*(6385), 204-208. https://doi.org/10.1126/science.aar3799

835

836 **Figure legends**

837 **Figure 1: *Epithelial type I and III interferon signaling mediate intestinal damage***
838 ***downstream of viral infection.*** **(A)** Survival of wildtype (WT; villin-cre^{-} littermate controls),
839 *Atg16l1*$^{\Delta IEC}$, *Atg16l1;Ifnlr*$^{\Delta IEC}$, *Ifnlr*$^{\Delta IEC}$, *Atg16l1;Ifnar*$^{\Delta IEC}$, and *Ifnar*$^{\Delta IEC}$ mice receiving 5% DSS in
840 drinking water for 6 days starting 10 days post inoculation (dpi) with MNV. **(B-C)** Cumulative
841 disease score (B) and weight loss (C) at day 6 post DSS from mice in (A). **(D)** Plaque forming
842 units (PFUs) of MNV per gram of stool from mice in (A) at 10 dpi. **(E-F)** Representative images of

843 ileal crypts stained for lysozyme (red) and DAPI (blue) (top) or for deoxynucleotidyl transferase–
844 mediated dUTP nick-end labeling (TUNEL) (bottom) of WT, *Atg16l1*$^{\Delta IEC}$, *Atg16l1;Ifnar*$^{\Delta IEC}$,
845 *Atg16l1;Ifnlr*$^{\Delta IEC}$, and *Atg16l1;Ifnlr;Ifnar*$^{\Delta IEC}$ mice infected with MNV on day 5 post DSS treatment
846 as in (A) (scale bars 20μm). **(F)** Violin plots depicting the repartition of the number of Paneth cells
847 observed in individual crypts, overlayed with symbols representing the average number of Paneth
848 cells per crypt observed in each mouse based on the lysozyme staining shown in (E). **(G)** Average
849 proportion of abnormal Paneth cells per crypt observed in each mouse as determined on the basis
850 of whether each Paneth cell displayed a typical staining pattern with distinguishable granules
851 (normal, orange arrow) or depleted and/or diffuse lysozyme staining (abnormal, white arrow) as
852 indicated in (E). **(H)** Proportion of crypts with 1, 2 or 3-5 TUNEL+ cells per mouse of each
853 genotype. Orange arrowheads indicate TUNEL^{+} cells in (E). At least 50 villi and crypts were
854 quantified per mouse. **(I)** Measurement of colon length from mice in (E-H). Each symbol
855 represents individual mice (or the mean in A) with bars representing mean ± SEM from at least
856 two independent experiments. Comparison between all genotypes was performed, not significant
857 comparisons are not indicated, *p≤0.05, **p≤0.01, ***p≤0.001, ****p≤0.0001, See also Figure S1.

858

859 **Figure 2: IFNβ and IFNλ2 exacerbate TNF-mediated cell death of intestinal organoids. (A)**
860 Representative images of small intestinal organoids derived from WT (*Atg16l1*$^{+/+}$)
861 and *Atg16l1*$^{\Delta IEC}$ mice (*Atg16l1*$^{-/-}$) cultivated in ENR medium for 3 days and stimulated for another
862 24h ± 20 ng/ml TNF, ± 100 U/ml IFNβ and ± 1ng/ml IFNλ2, then stained with Hoechst (blue) for
863 nuclei and propidium iodide (PI) (red) for cell death. Scale bars represent 1000 μm. **(B)** Viability
864 of *Atg16l1*$^{+/+}$ and *Atg16l1*$^{-/-}$ organoids stimulated with indicated cytokines over time as determined
865 by PI staining and organoid morphology. **(C)** Viability of organoids 48h post stimulation with 20
866 ng/ml TNF and 1 (low), 10 (med), 100 (high) U/ml IFNβ (left panel) or 0.01 (low), 0.1 (med), 1

867 (high) ng/ml IFNλ2 (right panel). **(D)** Quantification of TNF in culture supernatants by ELISA from
868 indicated organoids stimulated or not with 100 U/ml IFNβ for 48h. **(E)** Viability of *Atg16l1*$^{+/+}$ (left)
869 or *Atg16l1*$^{-/-}$ (right) organoids treated with 20 µg/ml anti-TNFα antibody or isotype control for at
870 least 30min before stimulation with cytokines. **(F)** Viability of *Atg16l1*$^{+/+}$, *Atg16l1*$^{-/-}$, *Atg16l1*$^{-/-}$*Ifnar*$^{-/-}$
871 (derived from *Atg16l1;Ifnar*$^{\Delta IEC}$ mice), and *Atg16l1*$^{-/-}$*Ifnlr*$^{-/-}$ organoids (derived from
872 *Atg16l1;Ifnlr*$^{\Delta IEC}$ mice) stimulated on day 3 for 48h. **(G)** Viability of organoids from the indicated
873 genotype stimulated 2h post seeding with 20 ng/ml TNF for 24 and 48h. For each condition, at
874 least 20 organoids were seeded in 3 different wells (technical triplicate), which was repeated in at
875 least 3 independent experiments with organoids derived from different mice each repeat. Each
876 symbol represents the average of one technical triplicate (or the mean for each stimulation in B)
877 with bars representing mean ± SEM. ns = not significant, *p≤0.05, **p≤0.01, ****p≤0.0001. See
878 also Figure S2.

879

880 **Figure 3: TNF and IFNλ synergize to promote RIPK1-dependent cell death in small**
881 **intestinal organoids. (A)** Representative images of Hoechst (blue) and PI (red) staining of small
882 intestinal organoids from WT (*Atg16l1*$^{+/+}$) and *Atg16l1*$^{\Delta IEC}$ mice (*Atg16l1*$^{-/-}$) cultivated in ENR
883 medium for 3 days and stimulated with ± 20 ng/ml TNF, ± 1ng/ml IFNλ2 for 48h. Organoids were
884 pre-treated with vehicle control, 100nM Ruxolitinib, 10µM Q-VD-OPh, or 10 µM Nec-1s for at least
885 30min before TNF+IFNλ2 stimulation. Scale bars represent 1000µm. **(B)** Quantification of
886 organoid viability from (A) at 24 and 48h post-stimulation. For each condition, at least 20
887 organoids were seeded in 3 different wells (technical triplicate), which was repeated in 3
888 independent experiments with organoids derived from different mice). **(C-E)** Representative
889 western blot of indicated proteins (C) and quantification of phosphorylated RIPK3 (pRIPK3) (D)
890 and cleaved caspase-3 normalized to β-actin and unstimulated control (E) in lysates from
891 *Atg16l1*$^{+/+}$ and *Atg16l1*$^{-/-}$ organoids stimulated for 2h with 20 ng/ml TNF alone or combined with

892 1ng/ml IFNλ2. C and FL designate cleaved and full length, respectively. **(F-G)** Representative
893 western blot of indicated proteins (F) and quantification of MLKL normalized to β-actin and
894 unstimulated control (G) in lysates from *Atg16l1*$^{+/+}$ organoids stimulated for 24h with 20 ng/ml TNF
895 alone, 1ng/ml IFNλ2 alone or the combination of both. **(H-I)** Viability of organoids derived from
896 WT and *Mlkl*$^{-/-}$ mice treated at day 3 with the indicated combinations of TNF, IFNλ2, and IFNβ for
897 24h (H) or 48h (I). Each symbol represents the average of one technical triplicate (B, I-J) or protein
898 expression observed from a pool of different wells in an independent experiment (F-H) with bars
899 representing mean ± SEM. ns = not significant, *p≤0.05, **p≤0.01, ****p≤0.0001. See also Figure
900 S2 and S3.

901

902 **Figure 4: *Virally-triggered intestinal disease in Atg16l1 mutant mice is RIPK3-dependent*.**
903 **(A)** Survival over time, cumulative disease score, and weight loss in *Atg16L1*$^{f/f}$, *Atg16L1*$^{\Delta IEC}$,
904 *Atg16L1*$^{f/f}$;*Ripk3*$^{-/-}$, and *Atg16L1*$^{\Delta IEC}$;*Ripk3*$^{-/-}$ mice infected for 10 days with MNV before receiving
905 3% DSS in their drinking water for 6 days. **(B)** Colon length on day 5 post DSS treatment of
906 indicated mice infected with MNV as in (A). **(C)** Representative images of H&E staining (top, scale
907 bar 100μm) and immunofluorescence of ileal crypts from mice in (B) stained for lysozyme (red)
908 and DAPI (blue) (bottom, scale bar 20μm). **(D)** Number of Paneth cells observed in each crypt in
909 mice from each genotype. **(E)** Average proportion of abnormal Paneth cells per crypt observed in
910 each mouse as determined on the basis of whether each Paneth cell displayed a typical staining
911 pattern with distinguishable granules (normal, orange arrow) or depleted and/or diffuse staining
912 (abnormal, white arrow). At least 50 crypts were quantified per mouse. Each symbol represents
913 individual mice with bars representing mean ± SEM from at least two independent experiments
914 (except for Paneth cell abnormality, n=1). ns = not significant, *p≤0.05, **p≤0.01, ***p≤0.001,
915 ****p≤0.0001.

916

917 **Figure 5: Intestinal organoids derived from *ATG16L1T300A* homozygous individuals**
918 **exhibit heightened susceptibility to inflammatory factors.** Organoids derived from human
919 small intestine biopsies were expanded in IntestiCult medium for several days before seeding in
920 differentiation medium to assess their viability. **(A-B)** Representative images at 24h post-
921 stimulation with ± 50 ng/mL hTNFα, ± 100 ng/mL hIFNλ2 (A) and viability over time (B) of
922 organoids from controls (n = 6 donors homozygous or heterozygous for the non-risk allele) and
923 *ATG16L1*^{T300A} homozygous individuals (n=3 donors). **(C)** Bar graph representation of data from
924 (B) comparing non-risk control and *ATG16L1*^{T300A} homozygous organoids. **(D-E)** Representative
925 pictures at 48h (D) and viability over time (E) of non-risk (n=3) and *ATG16L1T300A* homozygous
926 (n=3) organoids post incubation with pooled serum from healthy donors, patients with a blood
927 stream infection (BSI+ SARS-CoV-2-) or patients with a BSI and infected with SARS-CoV-2 (BSI+
928 SARS-CoV-2+). **(F)** Bar graph representation of data from (E) comparing non-risk control and
929 *ATG16L1*^{T300A} homozygous organoids. For each condition, at least 20 organoids were seeded in
930 3 different wells (technical triplicate). Each symbol represents the average viability per donor
931 across experiments (calculated from technical triplicates) with bars representing mean ± SEM for
932 each group. For (A-C) at least two independent experiments were performed for each organoid
933 donor. For (D-E), one experiment was performed for each organoid donor due to the limited
934 quantity of serum available. ns = not significant, *p≤0.05, **p≤0.01, ****p≤0.0001.

935

Figure 1

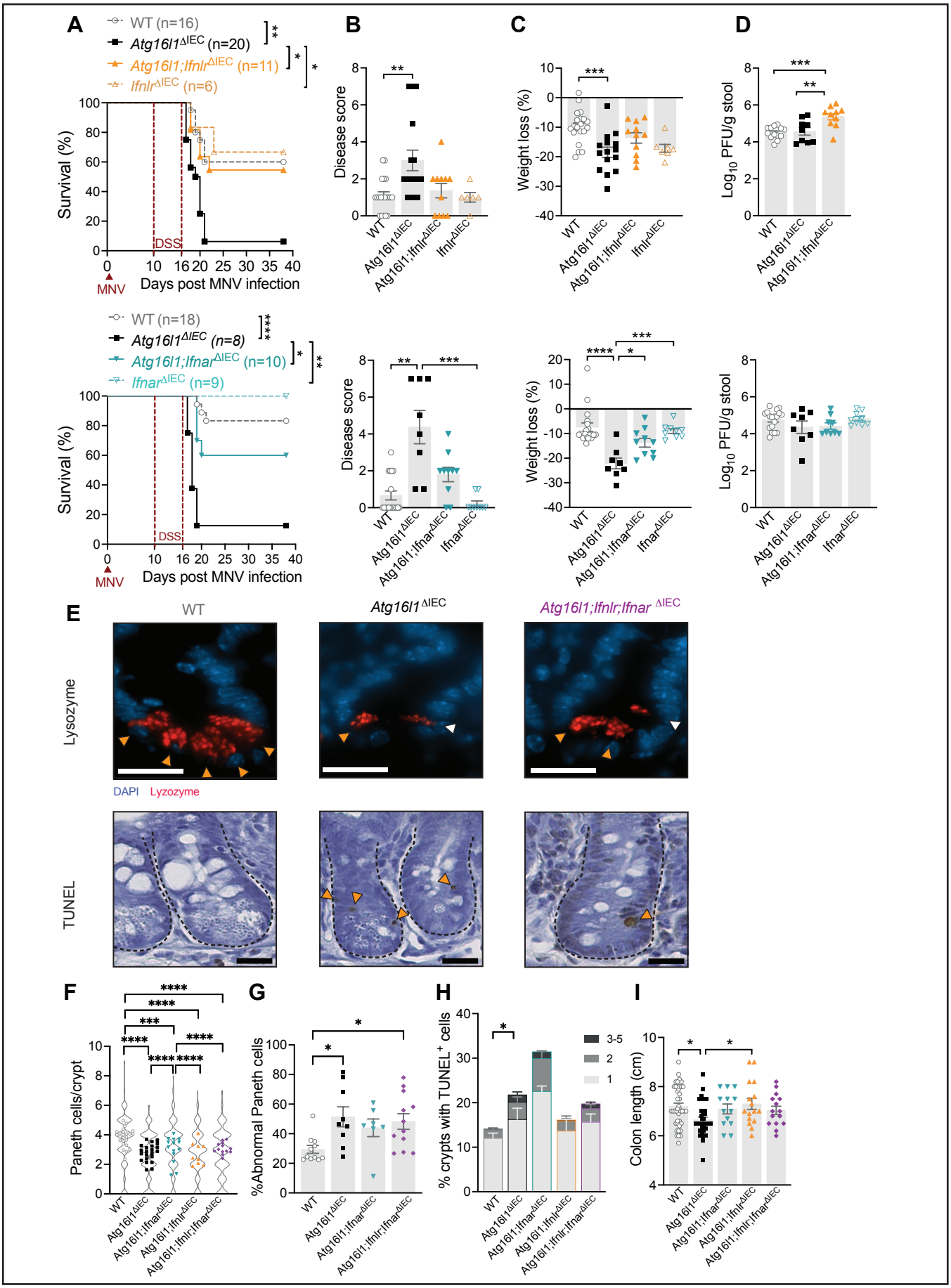
A
WT (n=16)
Atg16l1ΔIEC (n=20)
Atg16l1;IfnlrΔIEC (n=11)
IfnlrΔIEC (n=6)
Survival (%)
DSS
MNV
Days post MNV infection
B
Disease score
C
Weight loss (%)
D
Log10 PFU/g stool
WT
Atg16l1ΔIEC
Atg16l1;IfnlrΔIEC
IfnlrΔIEC
WT (n=18)
Atg16l1ΔIEC (n=8)
Atg16l1;IfnarΔIEC (n=10)
IfnarΔIEC (n=9)
Atg16l1;IfnarΔIEC
IfnarΔIEC
E
WT
Atg16l1 ΔIEC
Atg16l1;Ifnlr;Ifnar ΔIEC
Lysozyme
DAPI Lyzozyme
TUNEL
F
Paneth cells/crypt
G
%Abnormal Paneth cells
H
% crypts with TUNEL+ cells
3-5
2
1
I
Colon length (cm)
Atg16l1;Ifnlr;IfnarΔIEC

Figure 2

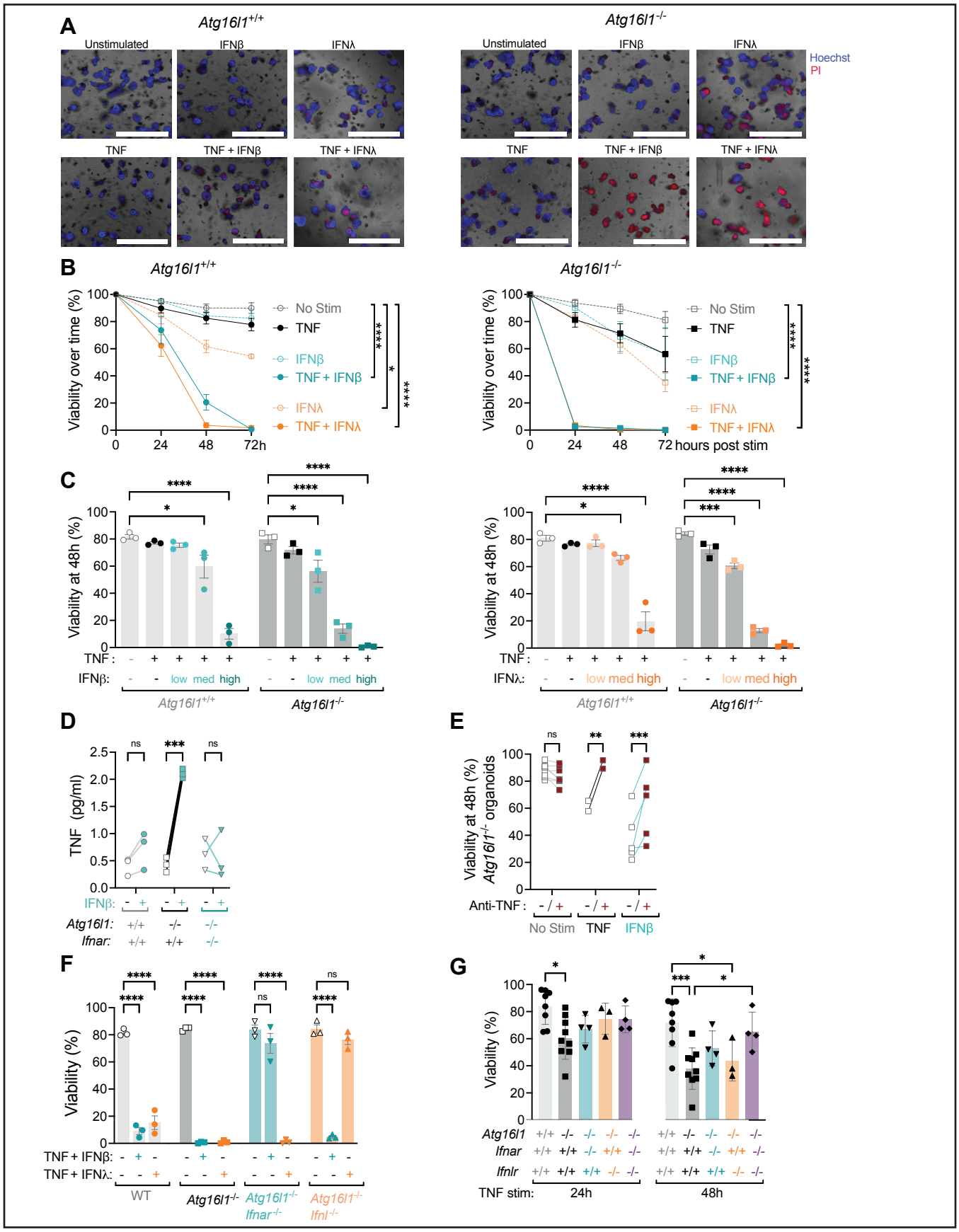
A
Atg16l1+/+
Atg16l1-/-
Unstimulated
IFNβ
IFNλ
TNF
TNF + IFNβ
TNF + IFNλ
Hoechst
PI
B
Viability over time (%)
No Stim
TNF
IFNβ
TNF + IFNβ
IFNλ
TNF + IFNλ
0 24 48 72h
0 24 48 72 hours post stim
C
Viability at 48h (%)
TNF :
IFNβ:
IFNλ:
low med high
Atg16l1+/+
Atg16l1-/-
D
TNF (pg/ml)
ns
***
IFNβ:
Atg16l1:
Ifnar:
E
Viability at 48h (%) Atg16l1-/- organoids
Anti-TNF :
No Stim
TNF
IFNβ
F
Viability (%)
TNF + IFNβ:
TNF + IFNλ:
WT
Atg16l1-/-
Atg16l1-/- Ifnar-/-
Atg16l1-/- Ifnlr-/-
G
Viability (%)
Atg16l1
Ifnar
Ifnlr
TNF stim:
24h
48h

Figure 3

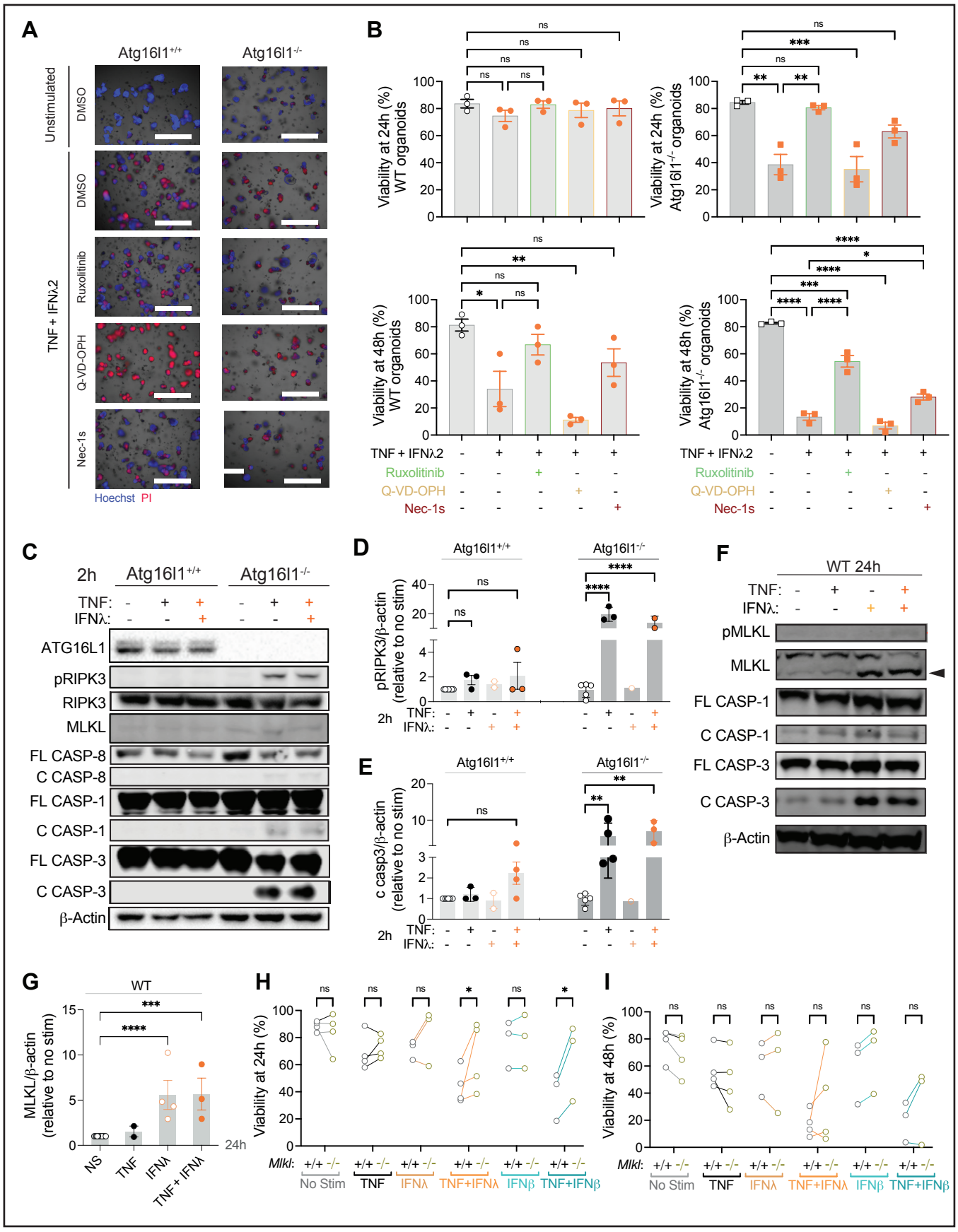
A
Atg16l1+/+
Atg16l1-/-
Unstimulated
DMSO
TNF + IFNλ2
DMSO
Ruxolitinib
Q-VD-OPH
Nec-1s
Hoechst PI
B
Viability at 24h (%) WT organoids
Viability at 24h (%) Atg16l1-/- organoids
Viability at 48h (%) WT organoids
Viability at 48h (%) Atg16l1-/- organoids
TNF + IFNλ2
Ruxolitinib
Q-VD-OPH
Nec-1s
C
2h
Atg16l1+/+
Atg16l1-/-
TNF:
IFNλ:
ATG16L1
pRIPK3
RIPK3
MLKL
FL CASP-8
C CASP-8
FL CASP-1
C CASP-1
FL CASP-3
C CASP-3
β-Actin
D
pRIPK3/β-actin (relative to no stim)
E
c casp3/β-actin (relative to no stim)
F
WT 24h
pMLKL
MLKL
FL CASP-1
C CASP-1
FL CASP-3
C CASP-3
β-Actin
G
WT
MLKL/β-actin (relative to no stim)
NS
TNF
IFNλ
TNF+IFNλ
24h
H
Viability at 24h (%)
Mlkl:
No Stim
TNF
IFNλ
TNF+IFNλ
IFNβ
TNF+IFNβ
I
Viability at 48h (%)

Figure 4

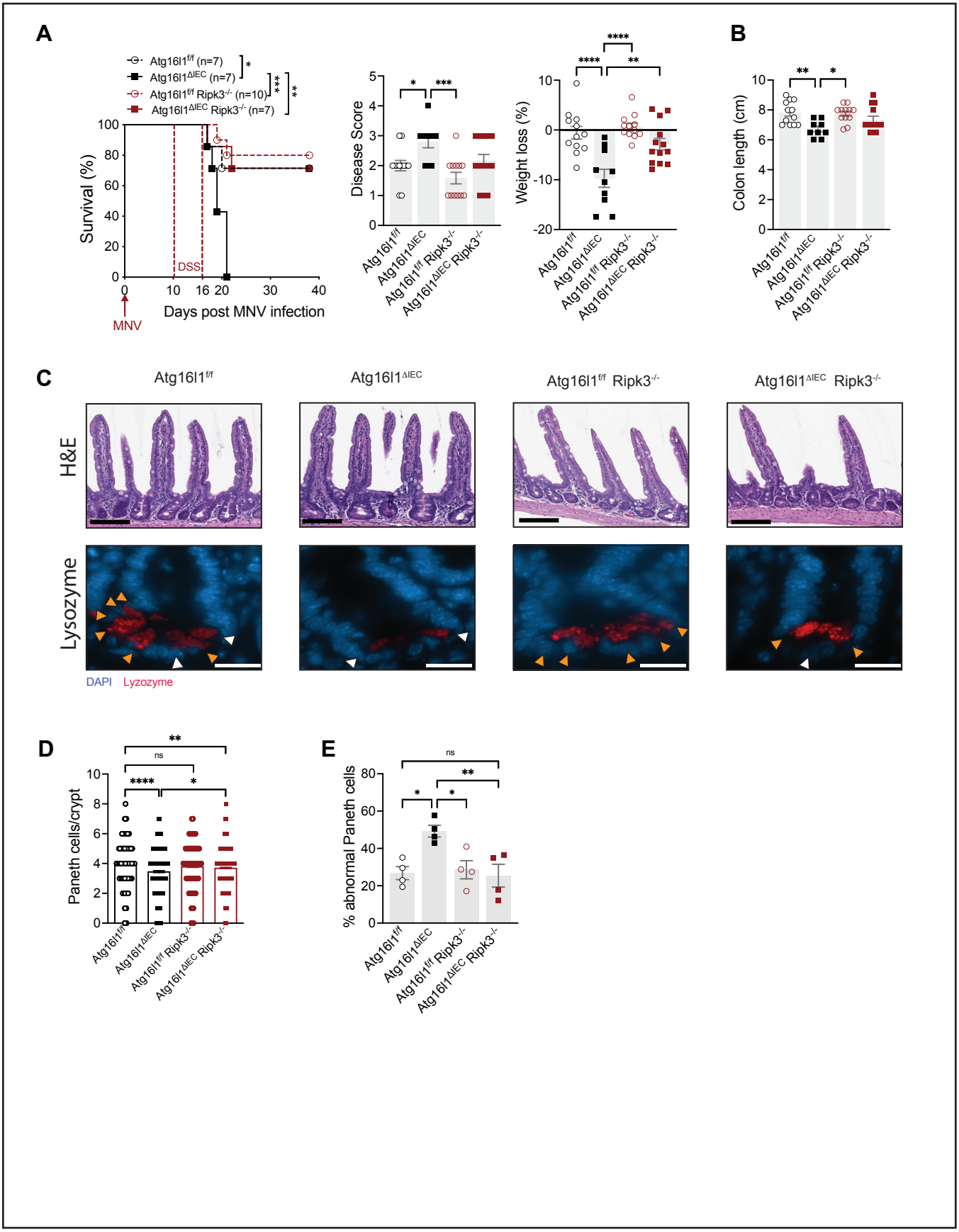
A
Atg16l1f/f (n=7)
Atg16l1ΔIEC (n=7)
Atg16l1f/f Ripk3-/- (n=10)
Atg16l1ΔIEC Ripk3-/- (n=7)
Survival (%)
DSS
MNV
Days post MNV infection
Disease Score
Weight loss (%)
B
Colon length (cm)
C
Atg16l1f/f
Atg16l1ΔIEC
Atg16l1f/f Ripk3-/-
Atg16l1ΔIEC Ripk3-/-
H&E
Lysozyme
DAPI Lyzozyme
D
Paneth cells/crypt
E
% abnormal Paneth cells

Figure 5

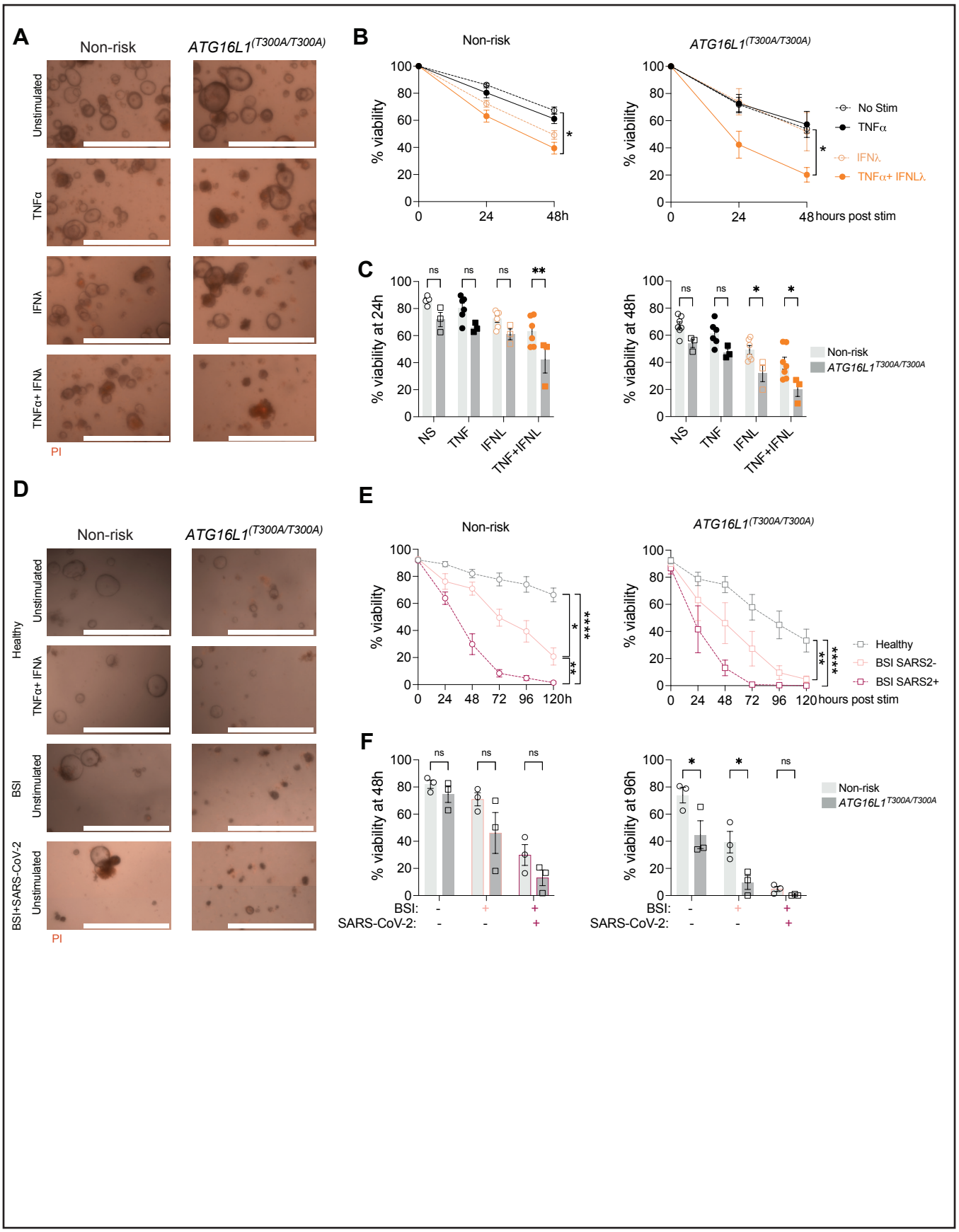
A
Non-risk
ATG16L1(T300A/T300A)
Unstimulated
TNFα
IFNλ
TNFα+ IFNλ
PI
B
Non-risk
ATG16L1(T300A/T300A)
% viability
hours post stim
No Stim
TNFα
IFNλ
TNFα+ IFNLλ
C
% viability at 24h
% viability at 48h
NS
TNF
IFNL
TNF+IFNL
Non-risk
ATG16L1T300A/T300A
D
Healthy
BSI
BSI+SARS-CoV-2
E
Healthy
BSI SARS2-
BSI SARS2+
F
% viability at 96h
BSI:
SARS-CoV-2: